

Study on the Ocean Colour Fluorescence Product

Product Validation Report

Date:
June 26, 2020

Prepared by :
Lena Kritten



Contents

1	Introduction	2
1.1	Scope of the document	2
1.2	Challenges for the validation of satellite based chlorophyll fluorescence	2
1.3	State of the Art	2
1.3.1	Correlation to in-situ chlorophyll	2
1.3.2	RTM studies on fluorescence	3
1.3.3	Other fluorescence products	3
1.3.4	Validation of MODIS and MERIS fluorescence	3
1.4	Product description	4
1.4.1	Radiance Fluorescence Peak Height (L-FPH)	5
1.4.2	Water-leaving-reflectance Fluorescence Peak Height (ρ_w -FPH)	5
1.4.3	Normalization	5
2	Validation	6
2.1	Validation approach	6
2.2	Validation against in-situ matchups	6
2.2.1	HPLC Matchup Database MDB	6
2.2.2	Transects in the Atlantic	9
2.2.3	In-situ Measurements in Lake Peipus	10
2.2.4	Conclusion on the comparison to in-situ matchups	12
2.3	Validation against OC4Me and Neural Network (NN) Chlorophyll from OLCI	15
2.3.1	Rio de la Plata	15
2.3.2	Black sea	19
2.3.3	Barents Sea	23
2.3.4	Conclusion on the comparison to OLCI standard chlorophyll	23
2.4	Validation against MODIS nFLH	27
2.4.1	Barents Sea, 5.7.2018, OLCI-B: 9:21am, MODIS AQUA: 8:40am	27
2.4.2	Namibian Coast, 25.11.2017, OLCI-A: 8:36am, MODIS AQUA: 12:34pm	30
2.4.3	German Bight, 26.8.2019, OLCI-A: 10:27am, MODIS AQUA: 12:13pm	33
2.4.4	Conclusion on the comparison to MODIS nFLH	35
2.5	Validation on simulated data	35
2.5.1	The RTM MOMO and the bio-optical model	35
2.5.2	Calculation of ρ_w and convolution to OLCI and MERIS spectral response function	37
2.5.3	BRDF effect	41
2.5.4	Conclusion on FPH simulations	43
3	Limitations	44
4	Conclusions	44

Table 1: Acronyms and Abbreviations

L_w	water-leaving radiance
nL_w	normalized water-leaving radiance
R_{rs}	remote-sensing-reflectance
F_0	extraterrestrial solar irradiance at mean Earth-Sun distance
$[\rho_w]_N$	normalized water-leaving reflectance
RTM	Radiative Transfer Model
RT	Radiative Transfer
L-FPH	Fluorescence Peak Height based on TOA radiance
ρ_w -FPH	Fluorescence Peak Height based on water-leaving reflectance
BRDF	Bidirectional Reflectance Distribution Function
θ_S	solar zenith angle
θ_V	viewing zenith angle
ϕ_V	viewing azimuth angle
srf	spectral response function
Chl	chlorophyll concentration

1 Introduction

1.1 Scope of the document

This document is the Product Validation Report (PVR) of the EUMETSAT Ocean Colour Fluorescence product (OC-Fluo) study and constitutes the study deliverable D-9. The goal of this document is to report on the validation datasets, methodologies and results. Once accepted by EUMETSAT this PVR will be also included in the OC-Fluo Algorithm Theoretical Basis Document (ATBD), section Validation. The authors acknowledge, that the word validation is used here, even though a full exhaustive validation should be based on more data and better statistics. This document includes a first evaluation of the product and the performance of the algorithm, as it was possible in the scope of the study.

1.2 Challenges for the validation of satellite based chlorophyll fluorescence

While validation is always a challenge, it is especially difficult in the case of measuring fluorescence from space. Remote sensing products are customarily validated against a ground truth. But Fluorescence is not an IOP, because it is not a property of the water body alone, but also a property of current and historical illumination. We do not have an independent ground truth for fluorescence, since this light emission is a response to photoinhibition, which is easily influenced by the in-situ measurement process. In-situ fluorescence measurements are governed by active light pulses and therefore not comparable to sun-induced fluorescence. The common approach to validate fluorescence from satellite based measurements is the comparison to chlorophyll concentration. Here, the strong correlation of chlorophyll fluorescence to chlorophyll concentration is employed, although the conversion of one measure to the other can vary by a factor of eight and there are a variety of factors influencing this.

1.3 State of the Art

1.3.1 Correlation to in-situ chlorophyll

The pure fluorescence signal does not only vary with variation in the chlorophyll-a pigment concentration, but is also affected by photoinhibition, phytoplankton species, and physiological states (Falkowski and Kiefer (1985); Mazeran et al. (2017)), and layering of phytoplankton.

Borstad et al. (1987) compiled FLH observations from several years and found that the relationship between FLH and chlorophyll could vary by a factor of eight. They also noted that the correlation within a particular study region was quite good and that the large variability only occurred when comparing different studies. In general, FLH varies from 0.01 to 0.08 W/m²/sr/mm per mg Chl. Lin et al. (2016) reports a strong diel cycle in in-situ measured fluorescence lifetime (which has a strong positive correlation to fluorescence efficiency), where the efficiency (lifetime) is higher at night than during daytime in spite of a marked increase under strong sunlight.

1.3.2 RTM studies on fluorescence

Using Radiative Transfer Modeling (RTM), Fischer and Kronfeld (1990) stated the sun-stimulated natural fluorescence of chlorophyll-a a good predictor for phytoplankton, even in waters with varying suspended matter and yellow substance concentrations. They found an increase in fluorescence of about 0.05 Wm⁻²sr⁻¹μm⁻¹ caused by an increase in chlorophyll concentration of 1 mgm⁻³, when a fluorescence efficiency factor of 0.3% was assumed. They also quantified the effect of vertical stratification.

1.3.3 Other fluorescence products

As of now, the most established fluorescence product, which is operationally available is the normalized Fluorescence Line Height (FLH) (Behrenfeld et al. (2009); Gower and King (2007a,b)). Here, a baseline is first formed by a linear interpolation of two baseline bands, and then subtracted from the radiance of the fluorescence band to obtain the FLH. The equation reads:

$$FLH = L_F - [L_R + (\lambda_R - \lambda_F)/(\lambda_R - \lambda_L)(L_L - L_R)] \quad (1)$$

where λ_F , λ_L , λ_R are the center wavelengths of the fluorescence band and the two baseline bands. L_F , L_L , L_R are the radiances of the fluorescence band and the two baseline bands. For MERIS, onboard ESA's satellite ENVISAT, the common combination is $\lambda_F = 681$ nm, $\lambda_L = 665$ nm, $\lambda_R = 709$ nm. For MODIS, onboard NASA's satellites Terra and Aqua, it is $\lambda_F = 678$ nm, $\lambda_L = 667$ nm, $\lambda_R = 748$ nm. For MODIS, the standard algorithm actually returns normalized Fluorescence Line Height (nFLH) in mW cm⁻² μm⁻¹ sr⁻¹, calculated as the difference between the observed nLw(678) and a linearly interpolated nLw(678) from two surrounding bands. Alternative algorithms use a simple reflectance ratio of the reflectance peak around 685 nm, e.g. reflectance at 670 and 560 nm (Xing et al., 2007).

1.3.4 Validation of MODIS and MERIS fluorescence

Hoge et al. (2003) conducted a validation of Terra-MODIS FLH using airborne laser-induced phytoplankton chlorophyll fluorescence data retrievals within Gulf Stream, continental slope, shelf, and coastal waters of the Middle Atlantic Bight portion of the western North Atlantic Ocean. From regression they derived a correlation coefficient of $r^2 = 0.85$. They conclude that the FLH methodology is equally valid within similar oceanic provinces of the global oceans. Huot et al. (2005) discuss important sources of variability in sun-induced chlorophyll fluorescence and examine difficulties in deriving fluorescence data products from satellite imagery, with a focus on MODIS. According to their findings MODIS FLH can be related to total fluoresced flux. Moreno-Madriñán and Fischer (2013) investigated the performance of the MODIS FLH algorithm in estuarine waters. They derived determination coefficients (r^2) at individual sites ranging between 0.67 (n=28, p<0.01) and no relationship, which means overall there is a not good relationship between in-situ chlorophyll-a and the FLH product ($r^2=0.20$, n=507) for these waters. Nevertheless, the low determination coefficient obtained was still eight times higher than that between in-situ chlorophyll-a and OC3M, the standard product traditionally used to estimate chlorophyll-a in ocean waters, which is based on the blue-green section of the spectrum. Gower and King (2007a) validated FLH from MERIS on the west coast of Canada. They present an average relation between FLH and surface chlorophyll concentration based on a simple model accounting for absorption of stimulating and emitted radiation by chlorophyll pigments, which gives a good

fit to the observations. They found a difference between the relation for offshore waters and those in coastal straits and inlets. This is in agreement with the findings of Gons et al. (2008), who documented the effective use of the MERIS FLH product in oligotrophic waters of the Laurentian Great Lakes, but failure (with FLH diminishing and becoming negative) in mesotrophic and eutrophic waters. Overall, we can assume that operational FLH algorithms that are based on the measurements of reflectance at three wavelengths in and around the fluorescence band, are sufficient for fluorescence retrieval in the open ocean where atmospheric correction algorithms work well and elastic reflectance in the fluorescence band is well approximated by the baseline curve due to the relatively weak elastic scattering signal which depends on [Chl] alone (Letelier (1996)). But this is not the case in coastal areas. Application of the FLH algorithms in the coastal waters is still significantly complicated by a peak in the underlying elastic reflectance which spectrally overlaps and contaminates any fluorescence retrieval. The structure and nature of this NIR peak is the result of a modulation of the particulate elastic spectrum (from both algal and non algal particles) by the combined phytoplankton and water absorption spectra, where the confluence of the decreasing phytoplankton absorption and the increasing absorption of water with wavelength results in a local absorption minimum. This absorption minimum leads to the maximum in the reflectance spectra which are inversely related to the total absorption.

Binding et al. (2011) even reported a moderate strength correlation ($R^2 = 0.57$) with a negative slope between FLH and in-situ chlorophyll at Lake of the Woods where chlorophyll concentration ranges between 2 - 70 mg/m^3 . As a reason they suggested that at this intensity of a bloom the absorption signal of chlorophyll dominates in the 681 nm band leading to a negative FLH. Ioannou et al. (2009) conclude that in order to compensate for the effects of this overlap of fluorescence and elastic spectra, and improve the operational FLH algorithms for coastal waters, it is clear that suitable models which attempt to take into account the larger impact of the spectral variation of the underlying elastic reflectance peak must be developed. They relate the ratio of the elastic reflectance components at 667 and 678 nm to that of the reflectance at 488 and 547 nm. These assist the new algorithm with a better performance in the quantification of chlorophyll in coastal waters compared to the standard FLH algorithms.

The relationship between chlorophyll-a and FLH is also complex due to variability in fluorescence quantum yield caused by taxonomic differences, phytoplankton physiology and light exposure history (Kiefer (1973); Letelier (1996)). Nonetheless, over the west Florida Shelf, Hu et al. (2005) established a robust relationship between MODIS FLH and in-situ chlorophyll-a that yielded superior estimates of chlorophyll-a compared with standard SeaWiFS or MODIS band-ratio chlorophyll-a. With this relationship, they were able to use FLH to differentiate between dark enhanced RGB features produced by high chlorophyll-a and those produced by high CDOM, thereby providing superior and more accurate feature identification than chlorophyll-a imagery. However, this technique was not developed for automatic detection and requires visual image interpretation.

Falkowski et al. (2017) present a statistical analysis of the correlation between measured in-situ fluorescence efficiency (lifetime) and satellite -derived estimates of the quantum yield of fluorescence, which shows a weak linear correlation. As possible reasons for this discrepancy, they give the noise of the satellite retrieved fluorescence signal for low open-ocean chlorophyll levels, pigment packaging and general uncertainties in the retrieval of satellite-based chlorophyll absorption coefficients. Still they recommend the use of quantum yields from ocean colour satellite retrievals in order to understand global physiology of phytoplankton. Gower (2014) even state, that satellite FLH does not need to be normalized with respect to SZA due to the existence of full stimulation over the relevant intensity range, or of quenching by an appropriately varying factor.

1.4 Product description

Within the framework of New Product Development, we investigated and developed a new Ocean Colour Fluorescence Product from Copernicus Sentinel-3 OLCI and implemented a product validation and review process. We aim to deliver an advanced and robust algorithm, that uses OLCI

spectral capabilities and ensures a high quality Fluorescence retrieval meeting user requirements in open ocean and complex waters. The concept of this fluorescence algorithm is to limit the analysis range to the red part of the spectrum and to approximate the Phytoplankton fluorescence peak and the secondary absorption peak with two Gaussian functions, while all other absorption and scattering processes are captured by a slope and an offset. The OC-Fluo algorithm delivers different products. Each is described separately here. The main products delivered from this study are L-FPH, if Level1 data is processed and ρ_w -FPH, if Level2 data is processed. By default implemented flags in the processor are the Level-2 WQSF flags: INVALID, LAND, CLOUD AMBIGUOUS, CLOUD.

Input	Bands	Processing Level	Description	Output	Description	Unit
L_{TOA}	Oa08-Oa12	Level-1B	spectral top-of-atmosphere radiance	L-FPH / L-APD	radiance Fluorescence Peak Height / radiance absorption peak depth	$\text{mWm}^{-2}\text{sr}^{-1}\text{nm}^{-1}$
ρ_w	Oa08-Oa12	Level-2	water-leaving reflectance / Surface directional reflectance, corrected for atmosphere and sun specular reflection	ρ_w -FPH / ρ_w -APD	water-leaving reflectance Fluorescence Peak Height / water-leaving reflectance absorption peak depth	-

Table 2: In- and output description of the OC-Fluo algorithm.

1.4.1 Radiance Fluorescence Peak Height (L-FPH)

L-FPH is the amplitude of the gaussian function, which is related to the fluorescence peak (centered at 681nm) that is fitted to Level-1 radiance (L_{TOA}). It is therefore a measure of the fluorescence signal in the TOA radiance spectrum. L-FPH is given in units of $\text{Wm}^{-2}\text{sr}^{-1}\text{nm}^{-1}$.

1.4.2 Water-leaving-reflectance Fluorescence Peak Height (ρ_w -FPH)

ρ_w -FPH is the amplitude of the gaussian function, which is related to the fluorescence peak (centered at 681nm) that is fitted to Level-2 water-leaving reflectance (ρ_w). It is a measure of the fluorescence signal in the water-leaving reflectance which is normalized by irradiance. Operational OLCI L2 reflectances are defined as the directional water surface reflectance, therefore ρ_w -FPH is dimensionless. The OLCI L2 products include the corrections for the Sun at zenith, the mean Earth-Sun distance, and the atmosphere. They do not include the BRDF corrections for viewing geometry, water optical properties, and the sky radiance distribution.

1.4.3 Normalization

Fluorescence products are customarily given in the unit of the processed quantity, because they measure the height or amplitude of the fluorescence peak in the measured spectrum. In order to put our fluorescence products in relation to the well-established normalized fluorescence line height (nFLH) of MODIS, we give here the corresponding equations. There are a number of steps in the normalization of water reflectances. The MODIS fluorescence algorithm returns nFLH in $\text{mW cm}^{-2}\mu\text{m}^{-1}\text{sr}^{-1}$, calculated as the difference between the observed normalized radiance at 678 nm ($\text{nLw}(678)$) and a linearly interpolated $\text{nLw}(678)$ from two surrounding bands

(Behrenfeld et al., 2009). The normalized water-leaving radiance is BRDF corrected. The relation between nLw and ρ_w is the following (Gordon and Voss, 1999):

$$\rho_w^N = \frac{\pi}{F_0} L_w^N = \frac{R/R_0 * \rho_w}{\cos(\theta_S) * t(\theta_S)} \quad (2)$$

While $\rho_w(\theta_S, \theta_V, \phi)$ can have different values for each combination of angles, ρ_w^N is per definition ρ_w at $\theta_S=0$ and $\theta_V=0$.

The presented ρ_w -FPH is based on OLCI's ρ_w , which includes the correction for the Sun at zenith, the mean Earth-Sun distance, and non-attenuating atmosphere. It does not include the BRDF correction for viewing geometry, water optical properties, and the sky radiance distribution. Whereas the presented L-FPH is based on L_{TOA} , which does not include any of the before-mentioned corrections, but is divided by a normalized F_0 in order to remove the interfering Fraunhofer lines.

2 Validation

2.1 Validation approach

The validation, as it could be performed in the scope of this study, is an evaluation of the algorithm and its products on different levels using multiple sources. Neither of the validations compares two identical measures.

1. Correlation with in-situ HPLC chlorophyll measurements
2. Correlation with standard OLCI chlorophyll products OC4me and NN
3. Inter-comparison with MODIS nFLH product (the only validation with another fluorescence measure)
4. Correlation with chlorophyll from RTM

As it is common practice for the validation of remote sensing products, the main validation of the Fluorescence products, L-FPH and ρ_w -FPH is performed through the comparison to in-situ measurements, but in this case, of chlorophyll concentration. The comparison to chlorophyll is state-of-the-art for the validation of fluorescence algorithms (see section 1.3). The fluorescence is expected in first order to be correlated to chlorophyll concentration. For the in-situ matchup comparison this chlorophyll concentration is the result of HPLC measurements. Additional to the default flags (see sec. 1.4), flags as recommended in EUMETSAT (2019) are applied for the validation against in-situ data (see section 2.2.1). Additionally, L-FPH and ρ_w -FPH are correlated to chlorophyll from the two standard operational Level-2 chlorophyll processors for OLCI, OC4me and Neural Network. Only in the comparison of L-FPH, ρ_w -FPH and MODIS nFLH two fluorescence measures are compared to each other. Finally ρ_w -FPH is compared to the input chlorophyll from RTM simulations.

2.2 Validation against in-situ matchups

2.2.1 HPLC Matchup Database MDB

The main data set for the validation of the OC-Fluo algorithm is the HPLC Matchup Database (MDB) which includes HPLC data from NASA SeaBASS Werdell et al. (2003) with OLCI matchups (Eumetsat Ocean Color In-situ Database, 2019) and is available at <https://ocdb.eumetsat.int/>. Most of the matchups are located in Santa Barbara Gulf in California (Pls David Siegel, Emmanuel Boss and Lynne Talley are gratefully acknowledged). Thus they are not representative for all kinds of waters, but they are very well distributed throughout seasons providing examples of different levels of chlorophyll-a concentration. The HPLC Matchups DataBase (HPLC MDB) is distributed by a netCDF file, providing both OLCI data (25 x 25 pixel centred over in-situ

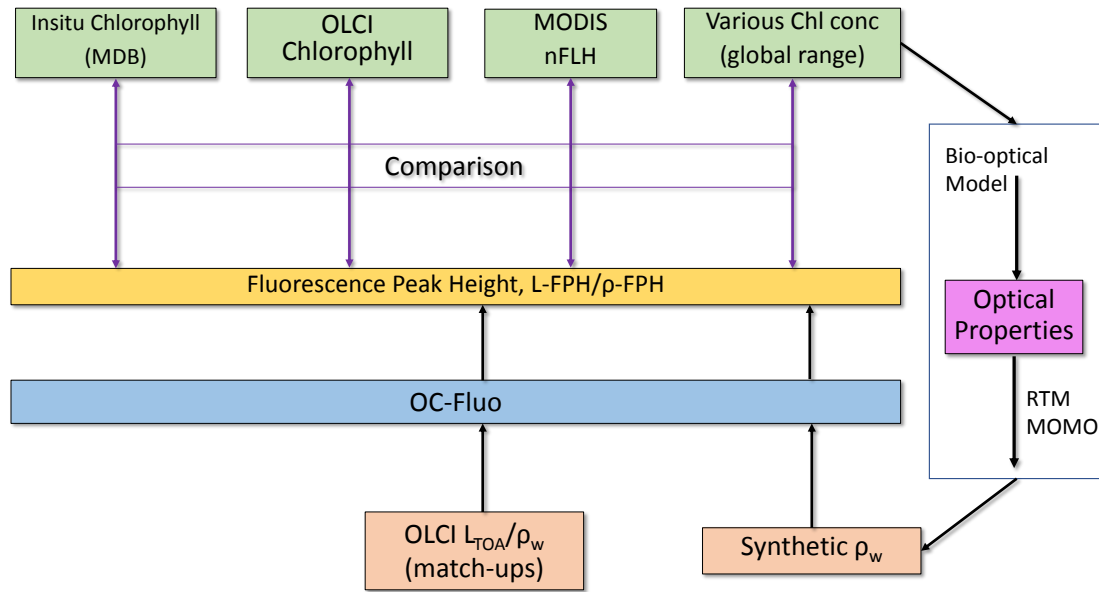


Figure 1: Validation approach for the OC-Fluo algorithm.

coordinates) and in-situ data. All variables are included as they are in the original OLCI Level-2 products. HPLC measurements are optically weighted to provide a unique value when multiple casts are provided within a radius of 150 m within 1 hour from the first measurement below the surface. A ± 3 -h window is assigned around the satellite overpass as condition for coincidence. Only in-situ measurements are included where at least one measurement in the top layer is available. For the satellite matchups, we follow the OLCI matchup protocol (EUMETSAT, 2019). A box of 5x5 pixels is defined, centered on the location of the in-situ measurement. This box allows for the generation of simple statistics, such as the mean and standard deviation, to assist in the evaluation of spatial stability, or homogeneity, at the validation point. On a pixel basis we applied the suggested Level-2 WQSF flags: CLOUD, CLOUDAMBIGUOUS, CLOUDMARGIN, INVALID, COSMETIC, SATURATED, SUSPECT, HISOLZEN, HIGHGLINT, SNOWICE, ACFAIL, WHITECAPS, ANNOTABSOD, ANNOTMIXR1, ANNOTTAU06, RWNEGO2, RWNEGO3, RWNEGO4, RWNEGO5, RWNEGO6, RWNEGO7, RWNEGO8, OC4MeFAIL. Only measurements are included where the sensor zenith is $< 60^\circ$ and sun zenith $< 70^\circ$. Fig. 2 shows a map with the locations of the remaining 30 valid HPLC measurements extracted from the SeaBASS database. In the Santa Barbara Gulf in California 22 measurements are made in the same area and cannot be separately displayed.

Fig. 3 shows the retrieved ρ_w -FPH and L-FPH from OLCI matchups over in-situ Chl concentration from global measurements. The white background shows the proposed sensitivity range.

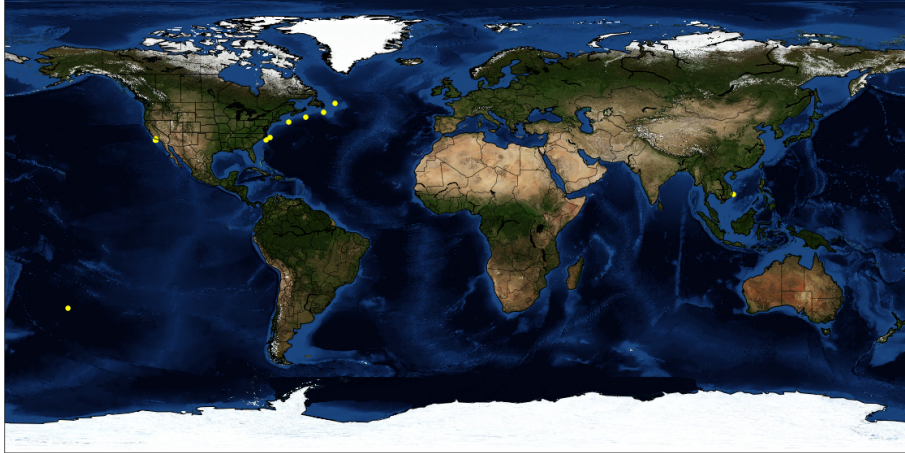


Figure 2: World map with locations of HPLC measurements extracted from SeaBASS database.

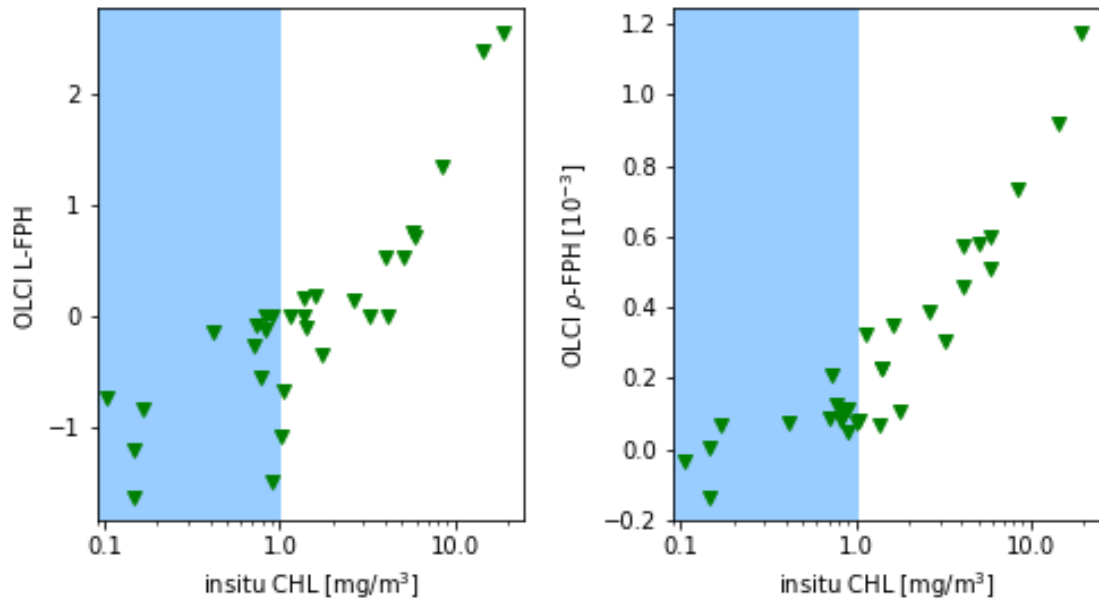


Figure 3: L-FPH from OLCI matchups over in-situ Chl concentration from HPLC measurements (left panel) and ρ_w -FPH from OLCI matchups over in-situ Chl concentration from HPLC measurements (right panel) from global measurements. The white background shows the proposed sensitivity range.

2.2.2 Transects in the Atlantic

The chlorophyll in-situ data from transects in the Atlantic Ocean are provided by Prof. Astrid Bracher, Alfred Wegener Institut, Germany. The water type here is mostly open ocean and the chlorophyll concentration is below the sensitivity range of the OC-Fluo algorithm. The data is shown here and used for validation purposes in order to show that low chlorophyll concentration does not produce unrealistic values but rather noise at lower values. Fig. 5 shows

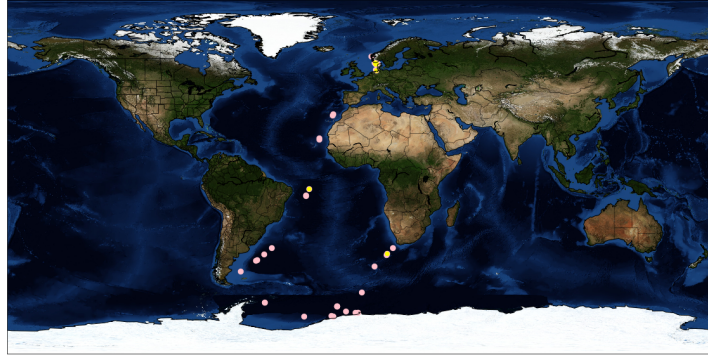


Figure 4: World map with locations of in-situ measurements from Astrid Bracher.

ρ_w -FPH and L-FPH over in-situ Chl concentration from transects in the Atlantic ocean. The in-situ chlorophyll concentration is mostly below the sensitivity range of the algorithm and the retrieved values are accordingly low.

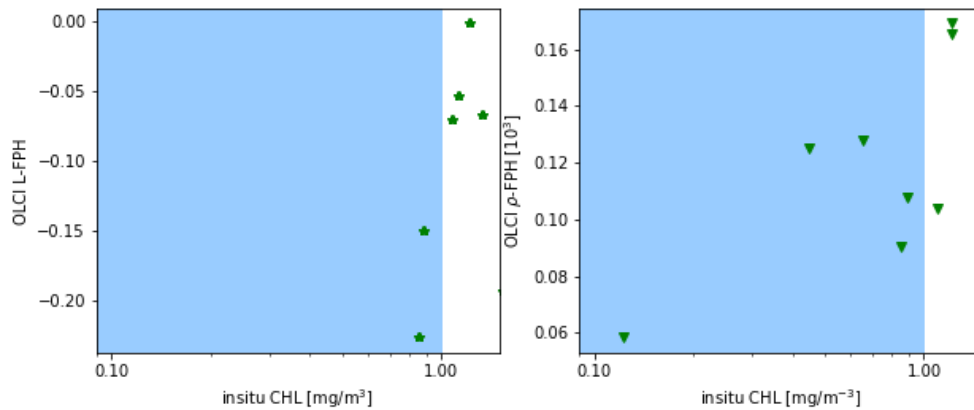


Figure 5: ρ_w -FPH from OLCI matchups over in-situ Chl concentration from HPLC measurements (left panel) and L-FPH from OLCI matchups over in-situ Chl concentration from HPLC measurements (left panel) from transects in the Atlantic. The white background shows the proposed sensitivity range.



Figure 6: Landsat satellite photo of Lake Peipus, from Wikipedia, 2019

2.2.3 In-situ Measurements in Lake Peipus

Lake Peipus is the largest transboundary lake in Europe, lying on the border between Estonia and Russia and the lake is the fifth-largest in Europe. Lake Peipus represents a remnant of a body of water which existed in this area during an Ice Age. It covers 3555 km², and has an average depth of 7,1 m, the deepest point being 15 m. The lake has several islands and consists of 3 parts:

- Lake Peipsi/Chudskoe, the northern part of the lake, with an area of 2611 km² (73%)
- Lake Pskov, the southern part of the lake (area 708 km² or 20%)
- Lake Lämmijärv/Teploe, the sound connecting the other two parts of the lake (area 236 km² or 7%)

The lake is used for fishing and recreation, but suffered from some environmental degradation from Soviet-era agriculture. Some 30 rivers and streams discharge into Lake Peipus. The largest rivers are the Emajõgi and the Velikaya River. The lake drains into the Gulf of Finland via the Narva River. The ecological condition of the lake basin is, in general, satisfactory – water is mostly of grades I and II (clean), and is of grade III in some rivers due to the high content of phosphorus. The water condition of the rivers has improved since 2001–2007, but there is an increase in population of blue-green algae. The main problem of Lake Peipus is its eutrophication, which generally increases from north to south.

We have access to in-situ measurements in Lake Peipsi of hyperspectral in-situ reflectances and chl-a from 2016 (courtesy of Krista Alikas, Tartu Observatory, Estonia). Chl was measured spectrophotometrically with a Hitachi U-3010 spectrophotometer and chlorophyll concentration was calculated according to the method of Jeffrey and Humphrey (1975).

Unfortunately there are no valid OLCI matchups when applying the criteria from the OLCI Matchup Protocols (EUMETSAT, 2019). Therefore, we process the in-situ reflectances and compare them to in-situ chlorophyll. When evaluating the in-situ reflectances many difficulties fall

away and the pure performance of the algorithm in complex waters can be tested. On the left side in Fig. 7 in-situ measured high resolution reflectance spectra are shown, from which the OC-Fluo retrieved ρ_w -FPH against chlorophyll from in-situ measurements is shown on the right side. For both dates ρ_w -FPH and chlorophyll show a very clear correlation, which is more linear in the case of the 27.7.16.

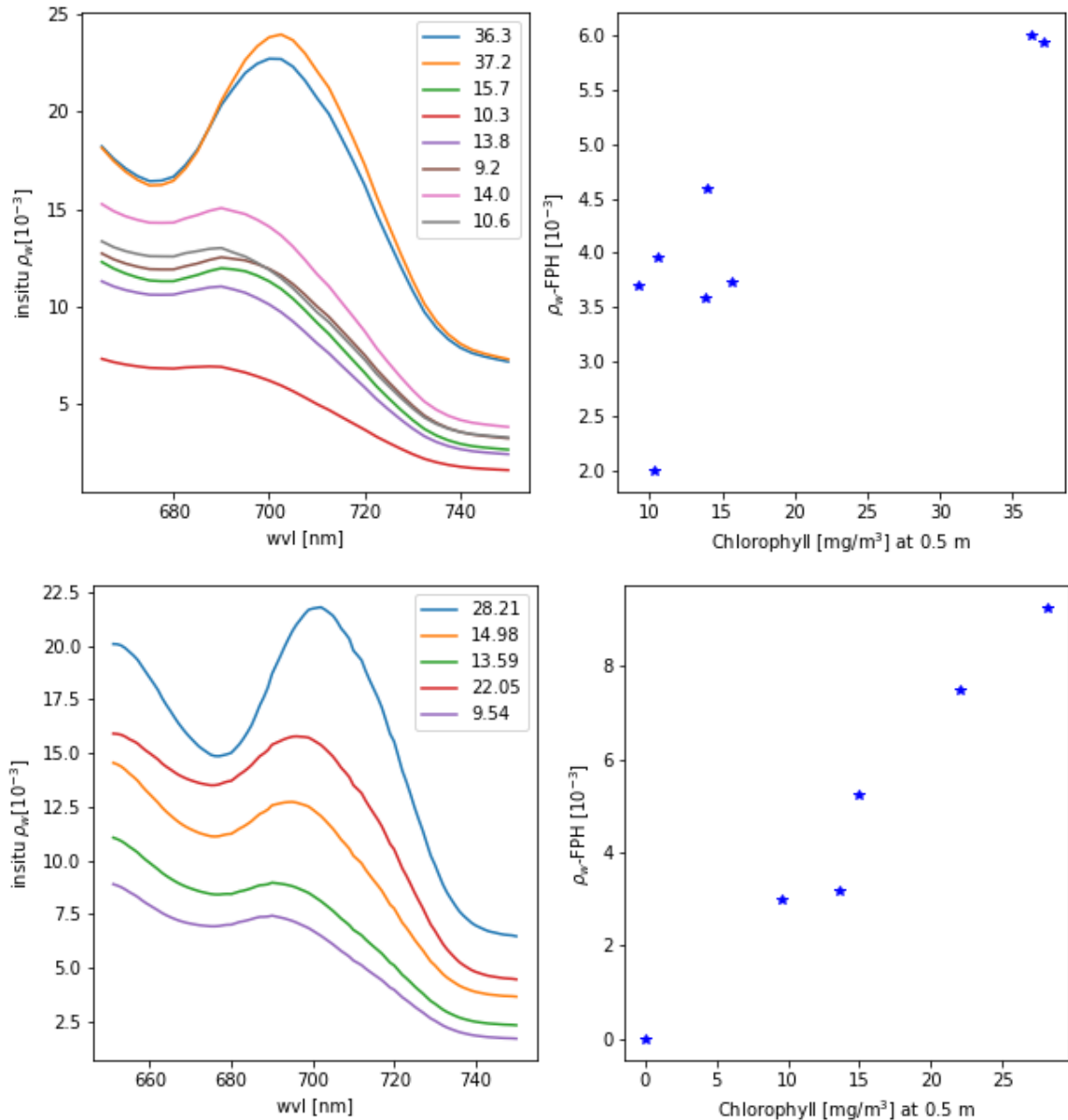


Figure 7: In-situ Rrs measured at Lake Peipus for different chlorophyll concentrations (left panel, numbers in mg/m³) for the 14.6.16 (upper panels) and the 27.7.16 (lower panels) and according ρ_w -FPH retrieved from the in-situ Rrs over chlorophyll concentrations from in-situ measurements (right panels).

Since the assumption of homogeneity is surely not given in this case and applying OLCI matchup protocols gives no valid output, we do not include this example into the validation of the OLCI fluorescence product but show this as an example of the ability of the algorithm to give an estimate of chlorophyll concentration in inland waters. However we process the OLCI data of the respective dates, where in-situ data is available. Fig. 8 shows OLCI L-FPH on the left side in colour code with overlaying Chl concentration in mg/m³ from the in-situ measurements

from the 14.06.2016 in Lake Peipsi and the same for ρ_w -FPH on the right side. Fig. 9 shows the same for the 27.07.2016. In both cases the gradient in chlorophyll concentration from the northern to the southern part of the lake is clearly represented by the FPH. Also finer structures are visible but do not clearly correspond to the in-situ measured chlorophyll values, which is probably due to the time lag between in-situ and satellite measurement and due to the heterogeneity in the lake. Close to the shore, adjacency effects might also play a role.

2.2.4 Conclusion on the comparison to in-situ matchups

As well L-FPH as ρ_w -FPH from OLCI matchups show a good correlation to global in-situ measured chlorophyll, if the chlorophyll concentration is higher than $1\text{mg}/\text{m}^3$. L-FPH obtain negative values for low chlorophyll concentration, which is most probably a negative offset due to atmospheric spectral influence. Because of the large scatter and negative values in FPH for $\text{Chl} < 1\text{mg}/\text{m}^3$, we define a sensitivity range for this algorithm of $\text{Chl} > 1\text{mg}/\text{m}^3$. Fitting this data with a polynomial function, we deduced a relation between FPH and chlorophyll, which is also part of the processor (see ATBD sec. 5).

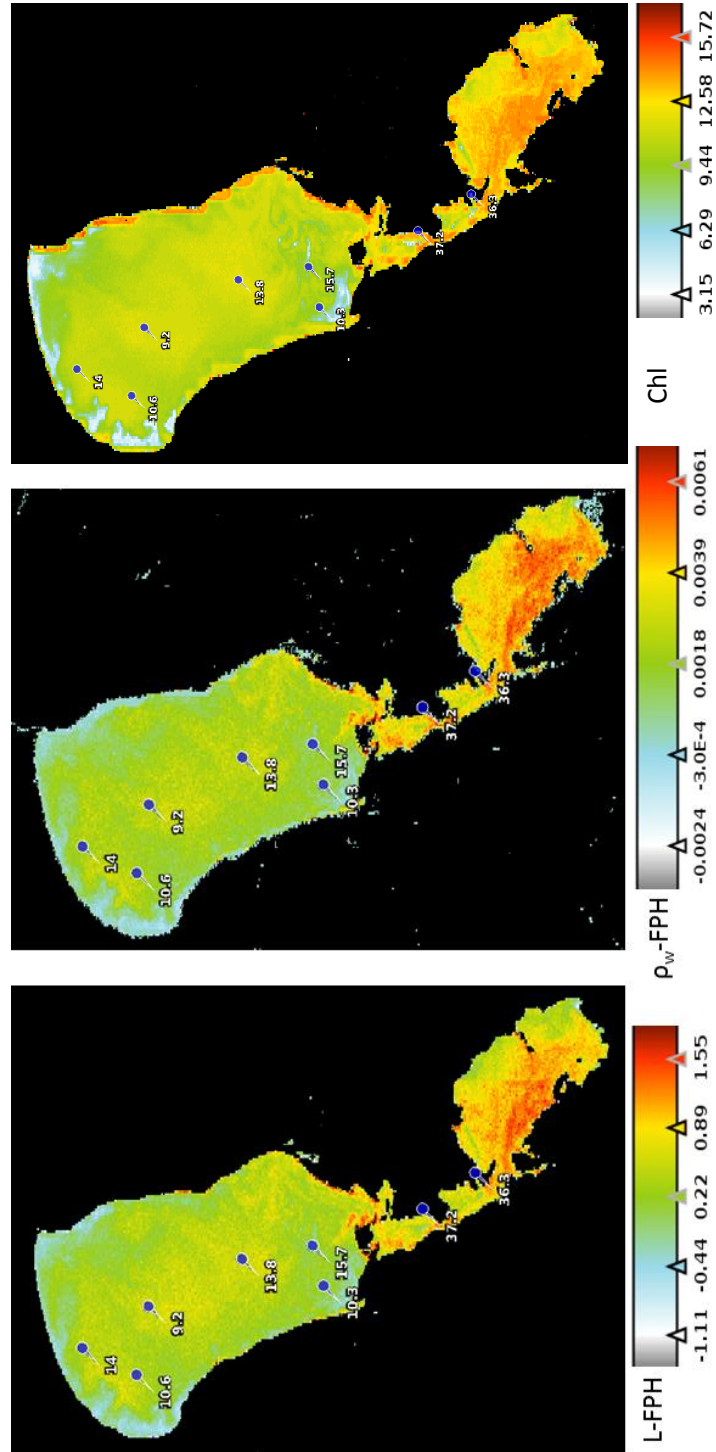


Figure 8: L-FPH (left panel) and ρ_w -FPH (middle panel) in Lake Peipsus retrieved by the OC-Fluo algorithm and NN chlorophyll (right panel) from OLCI data on 14.06.2016 (colour coded) and overlaying in-situ chlorophyll concentration in mg/m^3 .

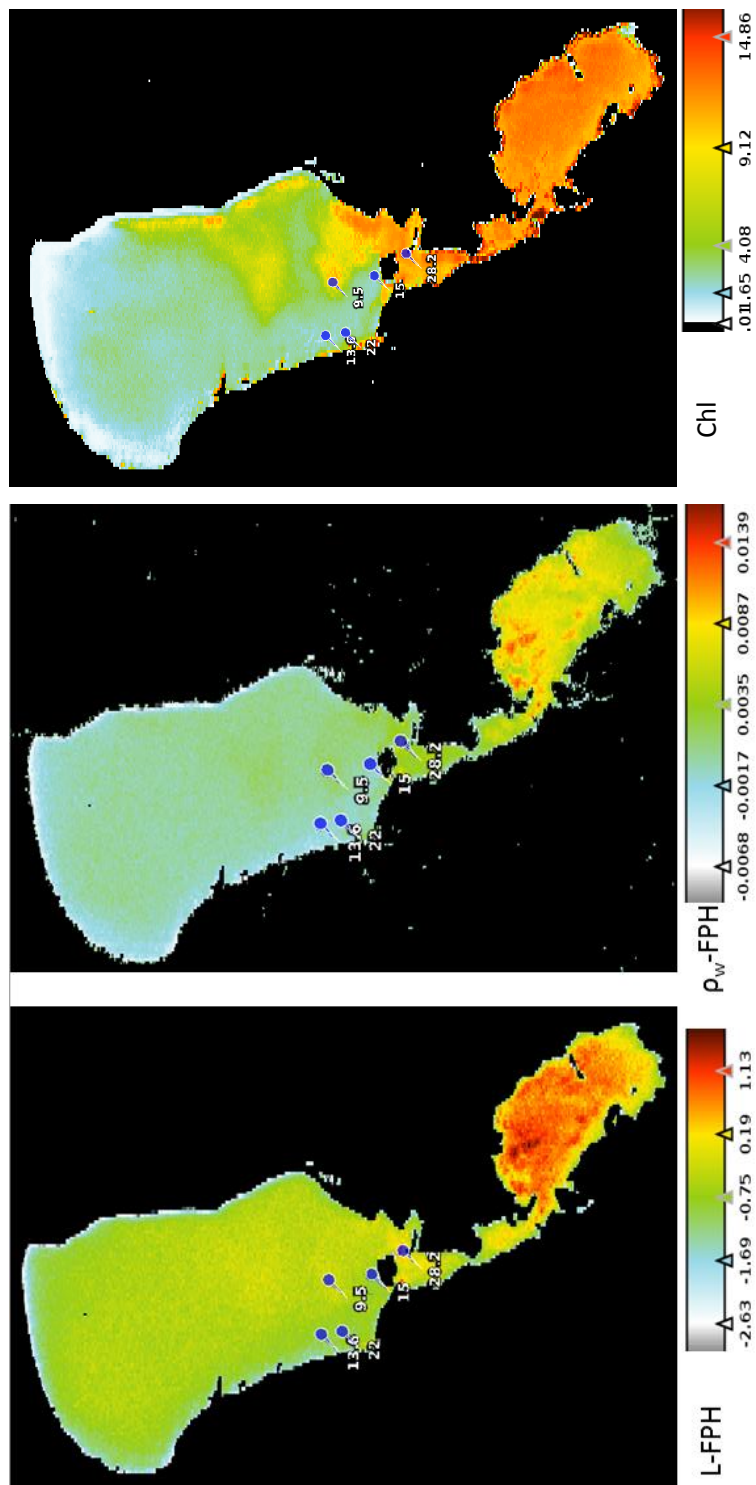


Figure 9: L-FPH (left panel) and ρ_w -FPH (middle panel) in Lake Peipsus retrieved by the OC-Fluo algorithm and NN chlorophyll (right panel) from OLCI data on 27.07.2016 (colour coded) and overlaying in-situ chlorophyll concentration in mg/m^3 from HPLC measurements at blue pins.

2.3 Validation against OC4Me and Neural Network (NN) Chlorophyll from OLCI

In this section we compare OC4Me and NN Chlorophyll with L-FPH and ρ -FPH by means of three example scenes with different water types. The NN Chlorophyll is estimated through an Inverse Modelling Technique based on an Inverse Radiative Transfer Model-Neural Network to estimate from normalised water-leaving reflectance at OLCI bands and among others the \log_{10} of the absorption coefficient of algal pigment from which Chl NN is derived (Brockmann et al., 2016). OC4Me is a Maximum Band Ratio semi-analytical algorithm, developed by Morel et al. (2007). For the comparison it is important to note, that the Neural Network Chlorophyll is more relevant for complex waters, whereas OC4Me is more appropriate in open ocean waters. The three scenes used in the validations are the Rio de la Plata estuary, part of the Barents Sea and a part of the Black Sea. The scenes are displayed with only the processors default flags (see sec. 1.4) applied. In order to derive a quantitative measure, we also derive a linear correlation coefficient R. A few studies show that on a local scale a linear relationship between fluorescence and chlorophyll concentration may exist (Fischer and Kronfeld, 1990), although other studies show that this relationship is strongly nonlinear (Babin et al., 1996). As a drawback of getting a good correlation and applying a simple general relationship, we derive the linear correlation coefficient R between FPH and the logarithm of Chl. Please note, that this coefficient is not necessarily a measure of the quality of the retrieval. For this pixel-wise correlation the OLCI matchup protocol (EUMETSAT, 2019) is applied.

2.3.1 Rio de la Plata

The South Atlantic Ocean near the Rio de la Plata Estuary is a highly dynamic and complex region that encompasses both Case 1 and Case 2 water types. This scene is characterized by extremely high, but also very low values of chlorophyll. Chlorophyll as a product from the OC4Me and NN processor on the 26th of November, 2017 is shown in Fig. 10. The concentration reaches from 0.1 mgm^{-3} in the open ocean to 25 mgm^{-3} in the estuary. L-FPH and ρ_w -FPH are shown in Fig. 11, also with highest values in the estuary. The patterns of L-FPH and ρ_w -FPH look similar to NN Chlorophyll, with an indication of a better resolution of high values for the FPH products. The correlation of L-FPH and ρ_w -FPH to Chlorophyll from OC4Me and NN is shown in Fig. 12. There is a clear correlation between FPH and NN Chlorophyll. Both, the correlation coefficient R between L-FPH and Chlorophyll from NN and Chlorophyll from OC4Me is 0.86. The correlation coefficient R between ρ_w -FPH and Chlorophyll from NN and Chlorophyll from OC4Me is 0.87.

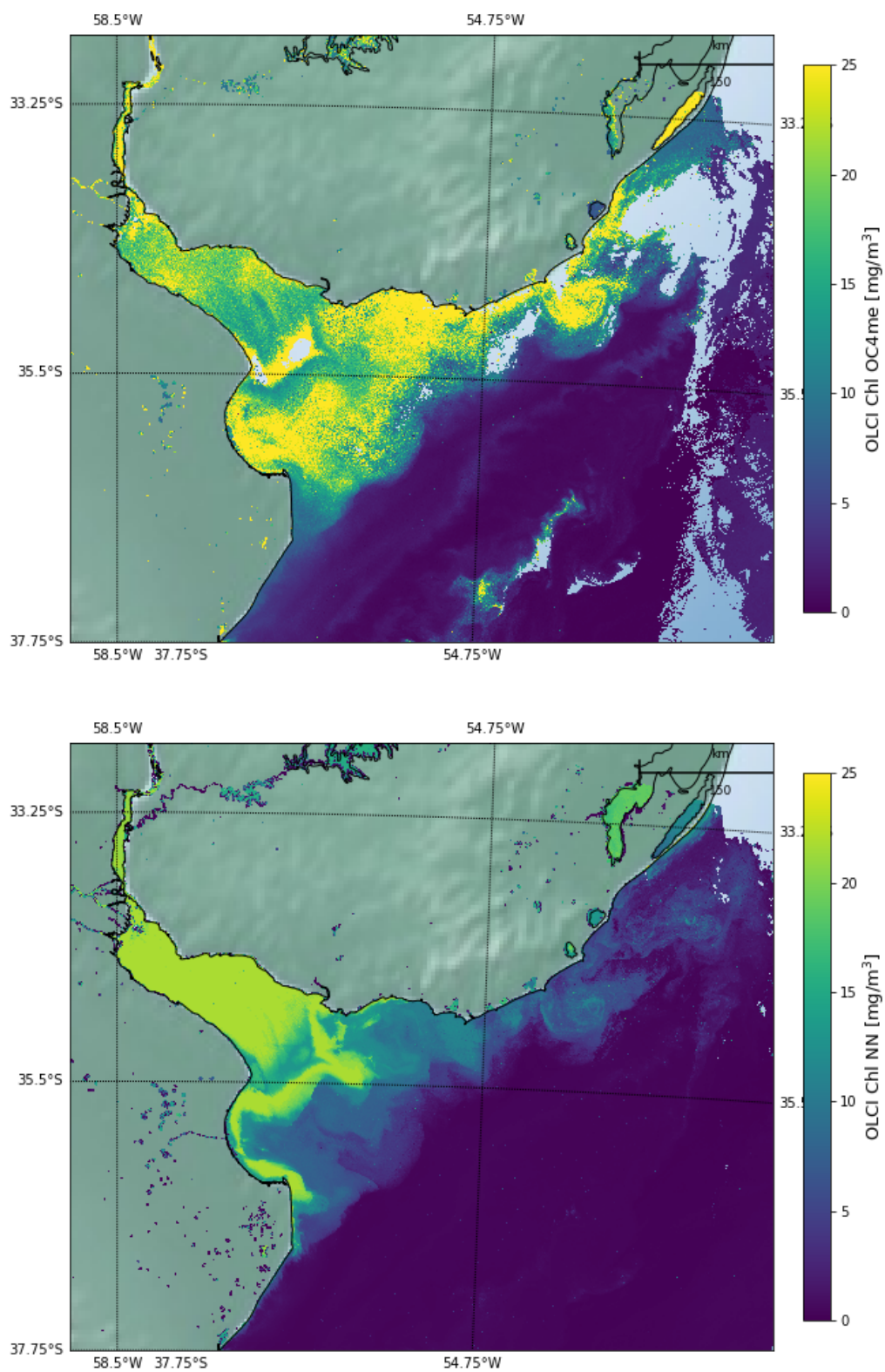


Figure 10: Chlorophyll Rio de la Plata from OC4Me (upper panel) and Neural Net processor (lower panel)

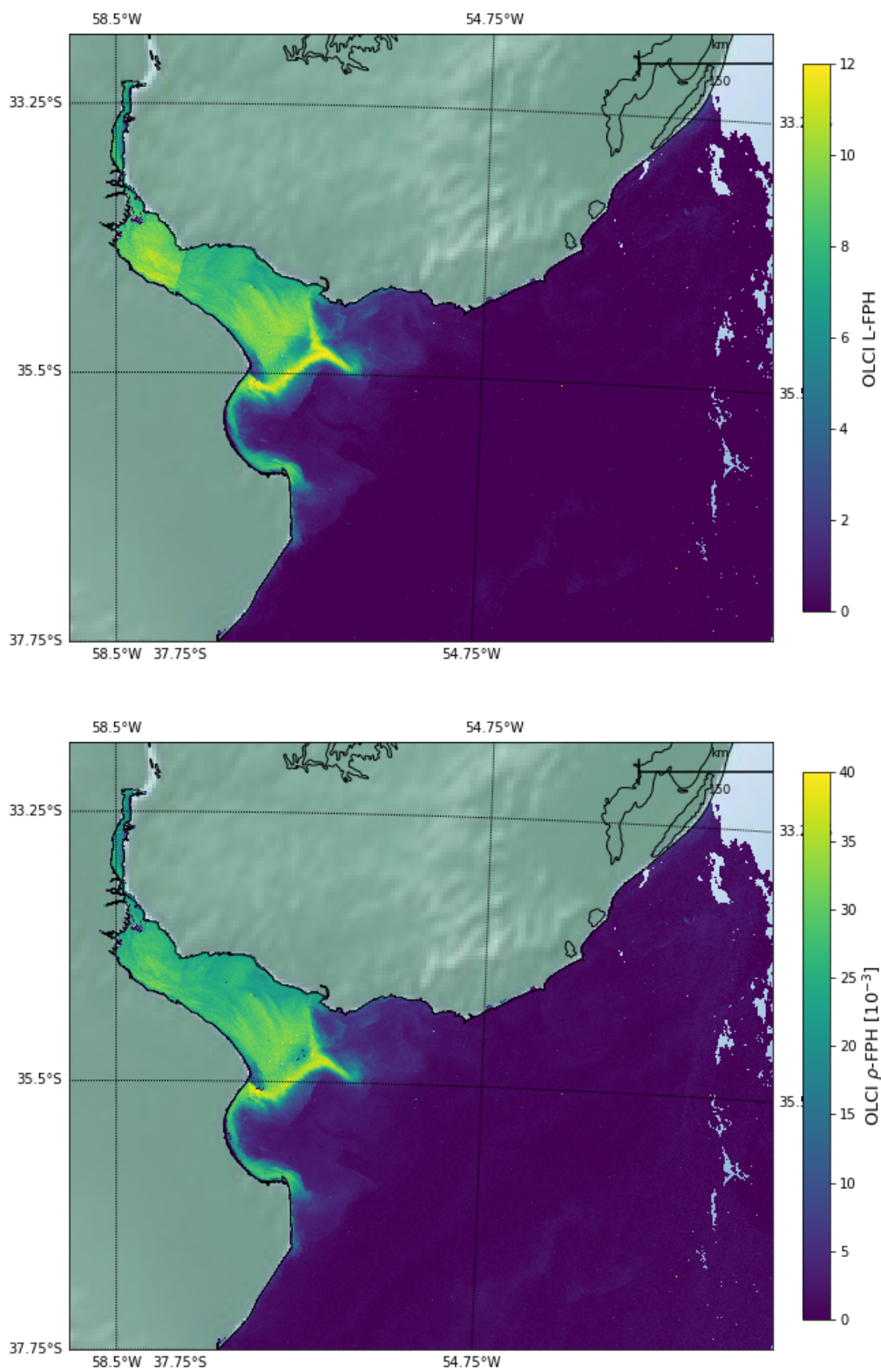


Figure 11: L-FPH (upper panel) and ρ_w -FPH (lower panel) at Rio de la Plata.

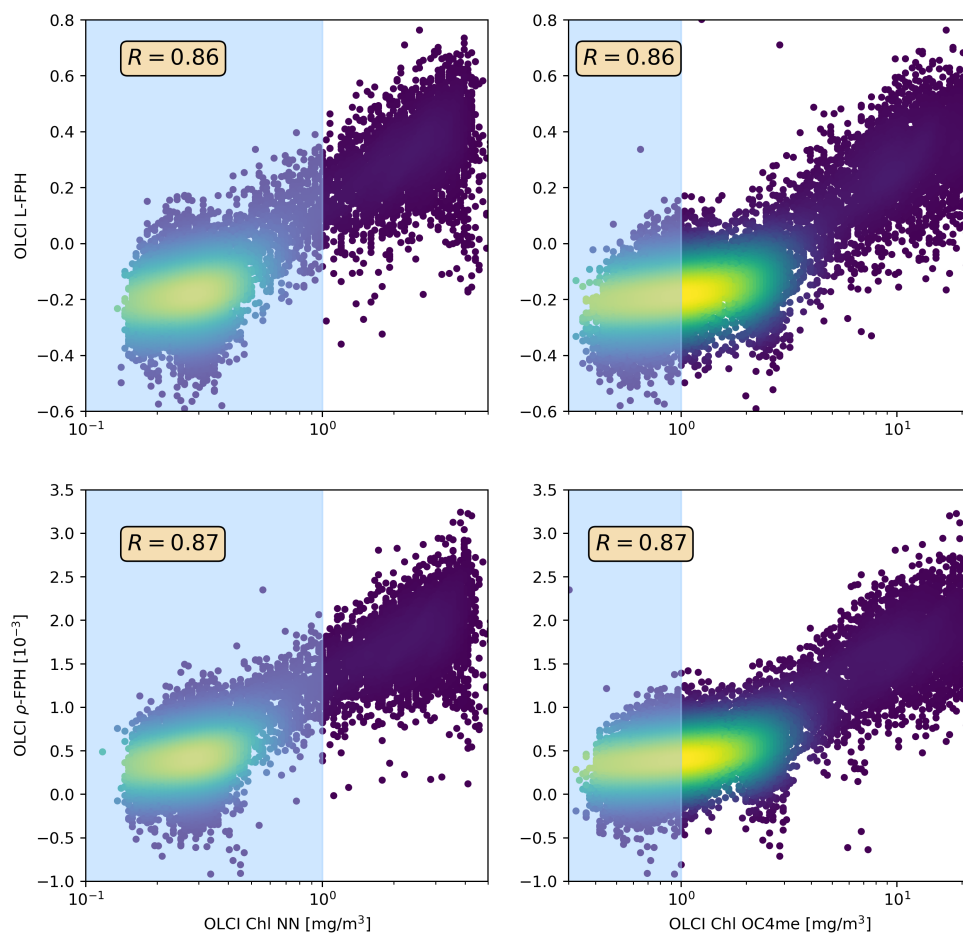


Figure 12: L-FPH and ρ_w -FPH against Chl from OC4Me (upper panel) and against Chl from NN in Rio de la Plata.

2.3.2 Black sea

The Black Sea lies between southeastern Europe and Asia Minor. Excluding its northern arm, the Sea of Azov, the Black Sea occupies about 168,500 square miles (436,400 square kilometers). It is connected to the Aegean Sea through the Bosphorus, the Sea of Marmara, and the Dardanelles (<https://www.ceoe.udel.edu/blacksea/geography/index.html>). The Chlorophyll concentration undergoes high seasonal and annual variability. Chlorophyll as a product from the OC4Me and NN processor on the 2nd of November, 2017 is shown in Fig. 13. The concentration reaches from 0.5 mgm^{-3} in the middle to 4 mgm^{-3} in the shelf regions, while the main portion is below 2 mgm^{-3} . At the shore OC4Me chlorophyll shows probably adjacency effects. L-FPH and ρ_w -FPH are shown in Fig. 14 and reveal patterns similar to the chlorophyll standard products. The correlation of L-FPH and ρ_w -FPH to Chlorophyll from OC4Me and NN is shown in Fig. 15. The correlation coefficient R between L-FPH and Chlorophyll from NN is 0.41 and Chlorophyll from OC4Me is 0.44. The correlation coefficient R between ρ_w -FPH and Chlorophyll from NN is 0.43 and Chlorophyll from OC4Me is 0.45. Depending on the processor for chlorophyll most or half of the pixels are outside of the sensitivity range of the FPH product.

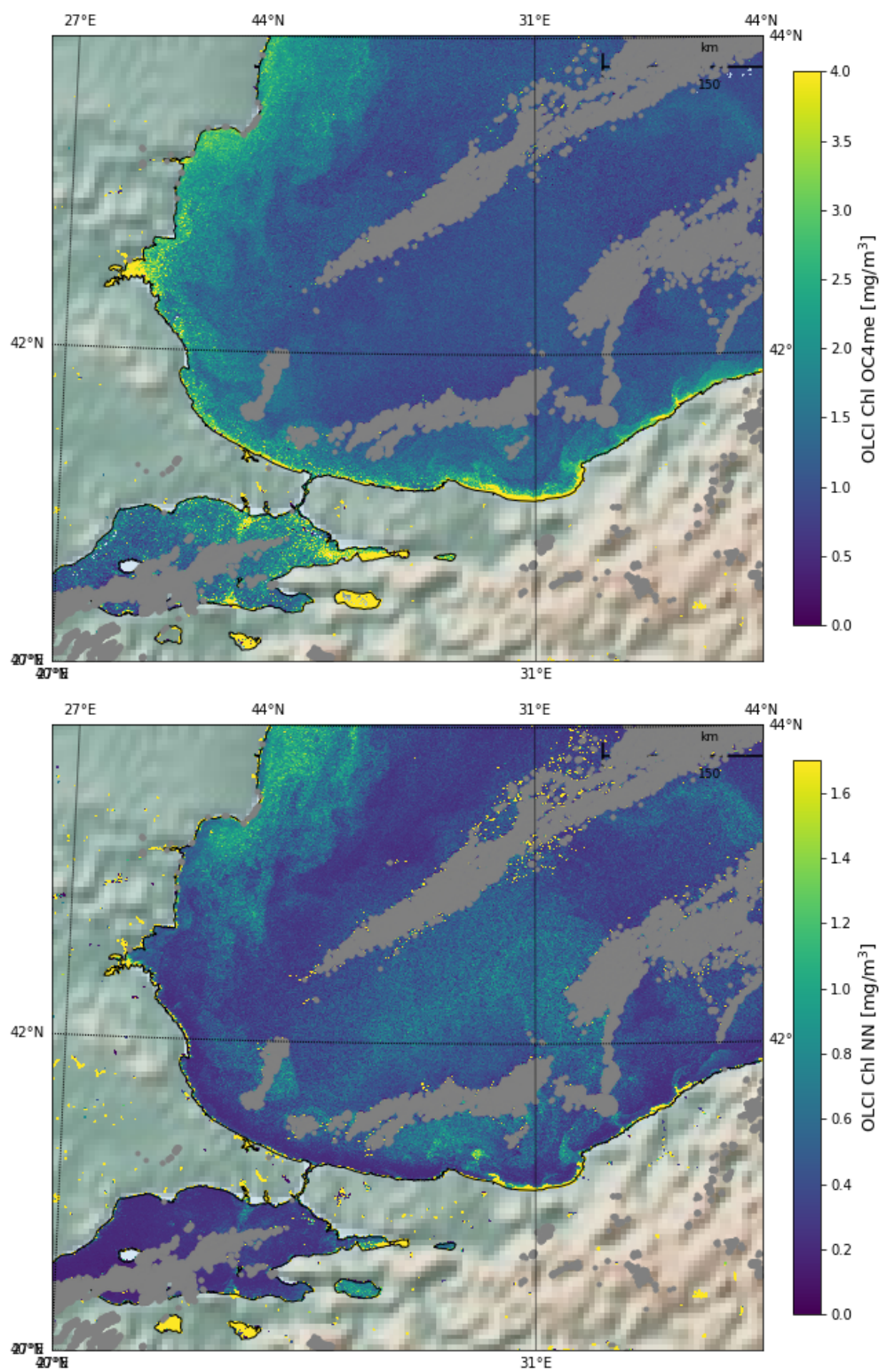


Figure 13: Chlorophyll Black Sea from OC4Me (upper panel) and Neural Net processor (lower panel)

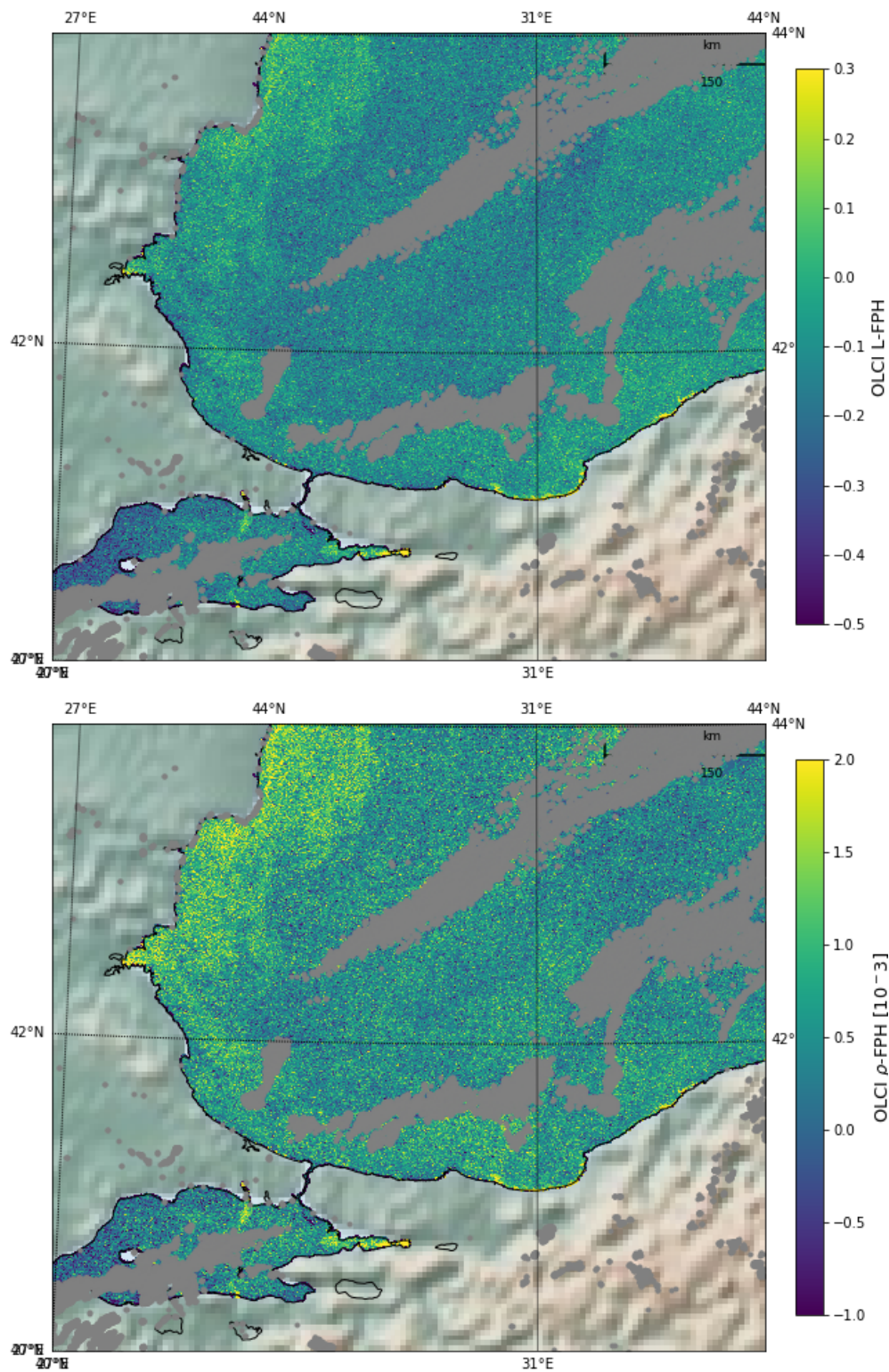


Figure 14: L-FPH (upper panel) and ρ_w -FPH (lower panel) in the Black Sea.

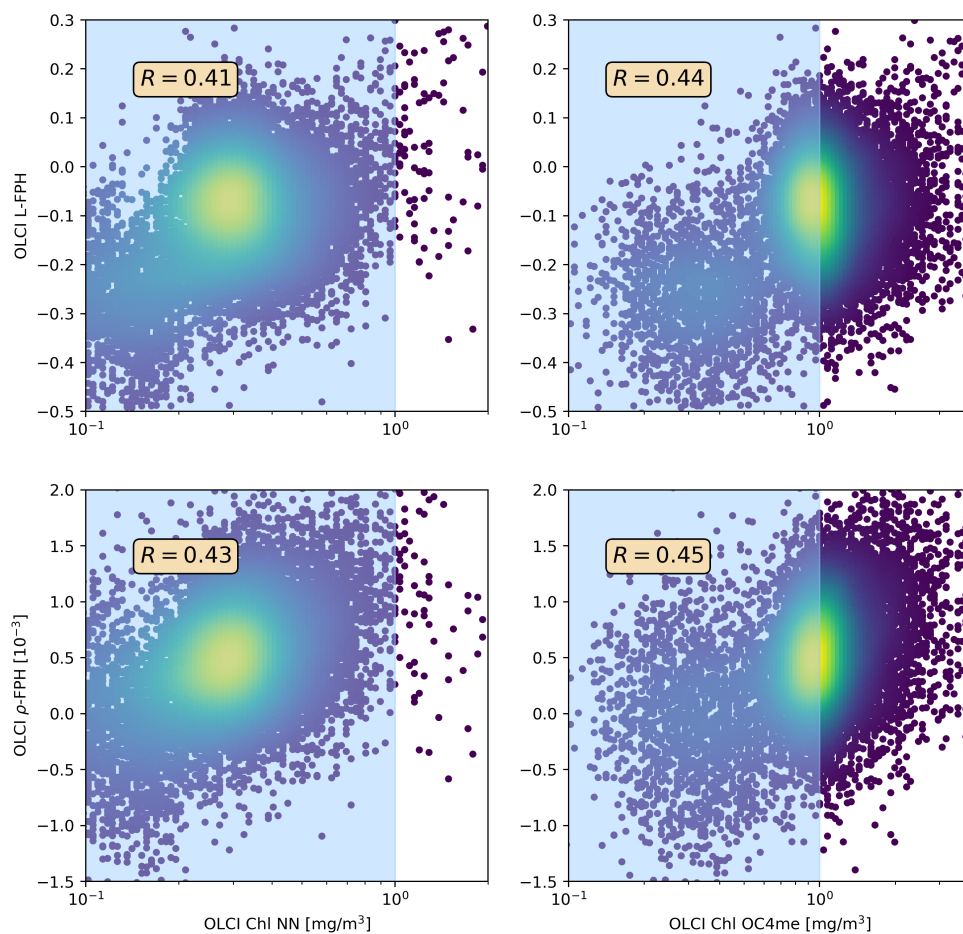


Figure 15: L-FPH and ρ_w -FPH against Chl from OC4me (upper panel) and against Chl from NN in the Black Sea.

2.3.3 Barents Sea

The Barents Sea is a marginal sea of the Arctic Ocean, located off the northern coasts of Norway and Russia and is divided between Norwegian and Russian territorial waters. It is a rather shallow shelf sea, with an average depth of 230 metres, and is an important site for both fishing and hydrocarbon exploration. Despite being part of the Arctic Ocean, the Barents Sea has been characterised as "turning into the Atlantic" because of its status as "the Arctic warming hot spot." Hydrologic changes due to global warming have led to a reduction in sea ice and in stratification of the water column, which could lead to major changes in weather in Eurasia. Due to the North Atlantic drift, the Barents Sea has a high biological production compared to other oceans of similar latitude. The spring bloom of phytoplankton can start quite early close to the ice edge, because the fresh water from the melting ice makes up a stable water layer on top of the sea water.

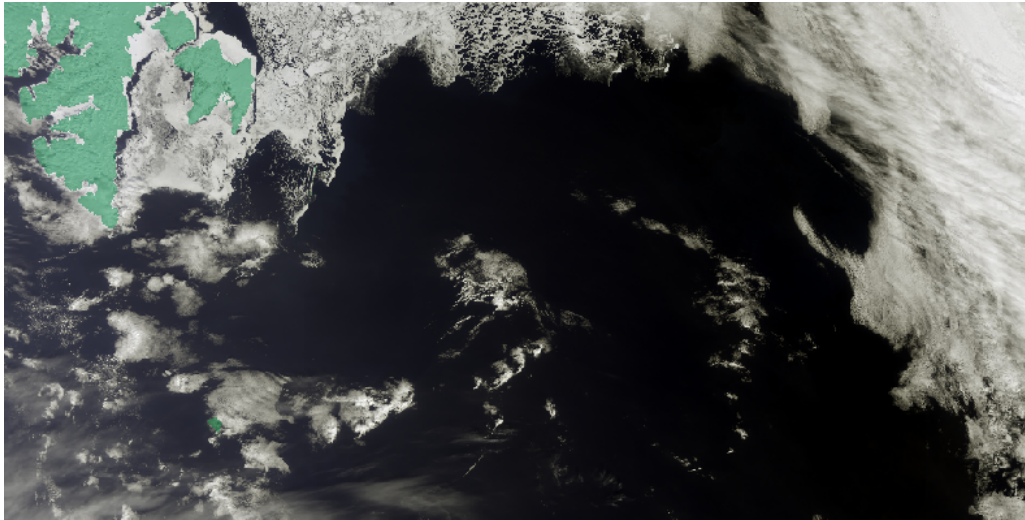


Figure 16: RGB, OLCI Level-1b, Barents Sea.

Fig. 17 and 18 show L-FPH and ρ_w -FPH and OC4Me and NN Chlorophyll on the 7th of May, 2018 in the Barents Sea. L-FPH and ρ_w -FPH reveal distinctive patterns, which are very similar to the patterns detected as NN chlorophyll. The correlation of L-FPH and ρ_w -FPH to Chlorophyll from OC4Me and NN is shown in Fig. 19. Both, the correlation coefficient R between L-FPH and Chlorophyll from NN and Chlorophyll from OC4Me is 0.79. The correlation coefficient R between ρ_w -FPH and Chlorophyll from NN is 0.76 and Chlorophyll from OC4Me is 0.80.

2.3.4 Conclusion on the comparison to OLCI standard chlorophyll

As well L-FPH as ρ_w -FPH show an overall good correlation to OC4me and NN chlorophyll above a concentration of around $1\text{mg}/\text{m}^3$.

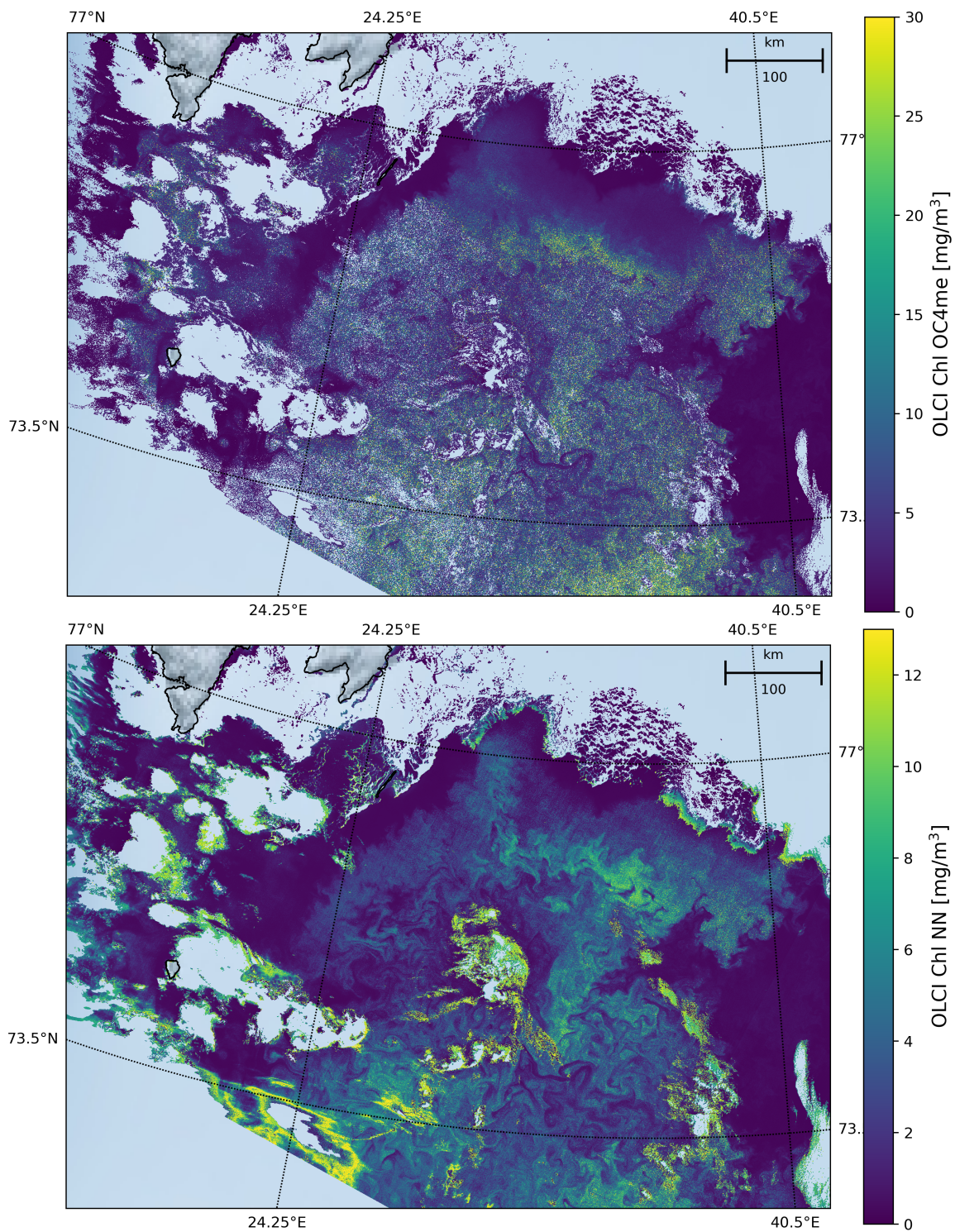


Figure 17: Chlorophyll in the Barents Sea from OC4Me (upper panel) and Neural Net processor (lower panel)

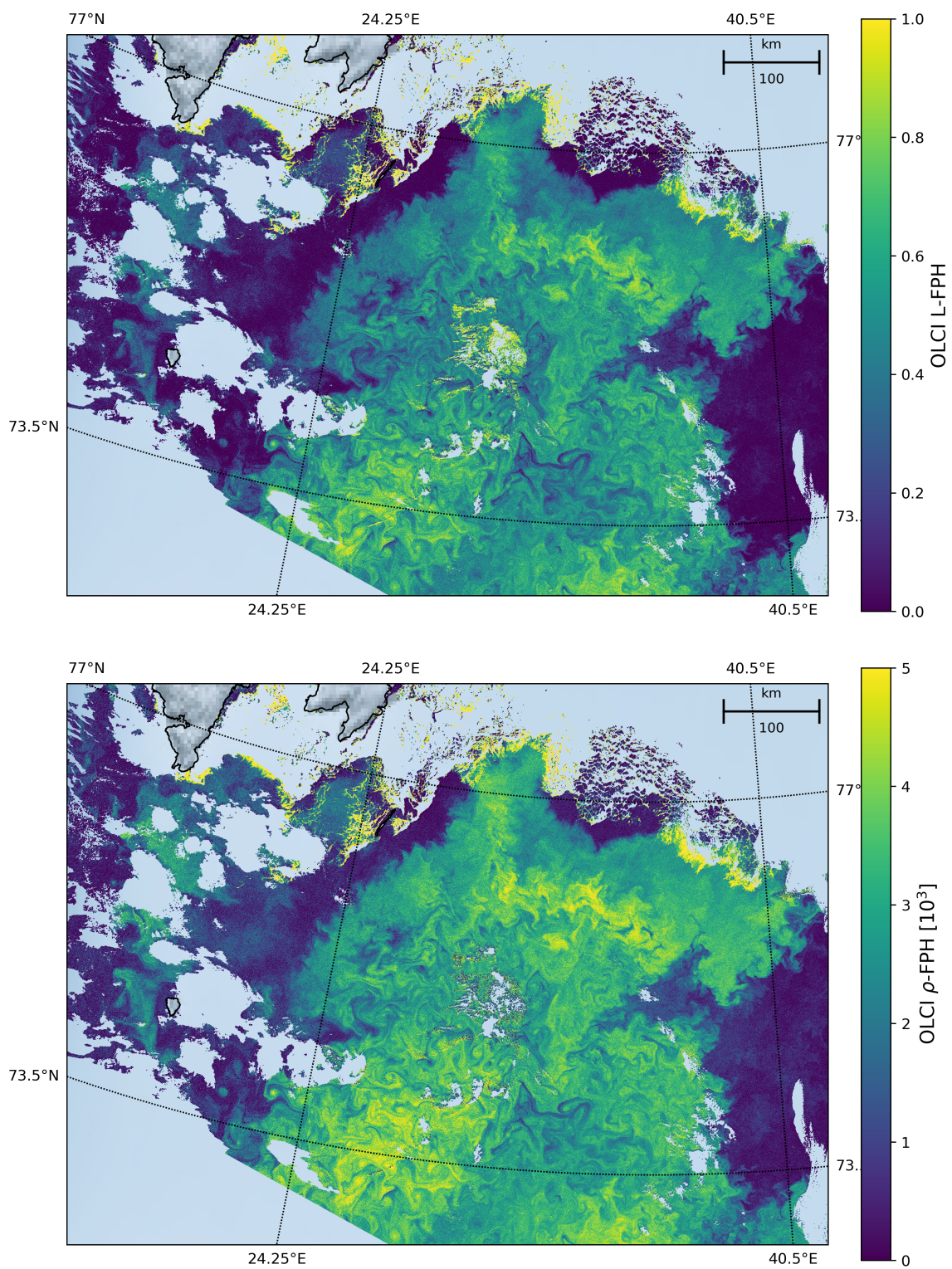


Figure 18: L-FPH (upper panel) and ρ_w -FPH (lower panel) in the Barents Sea.

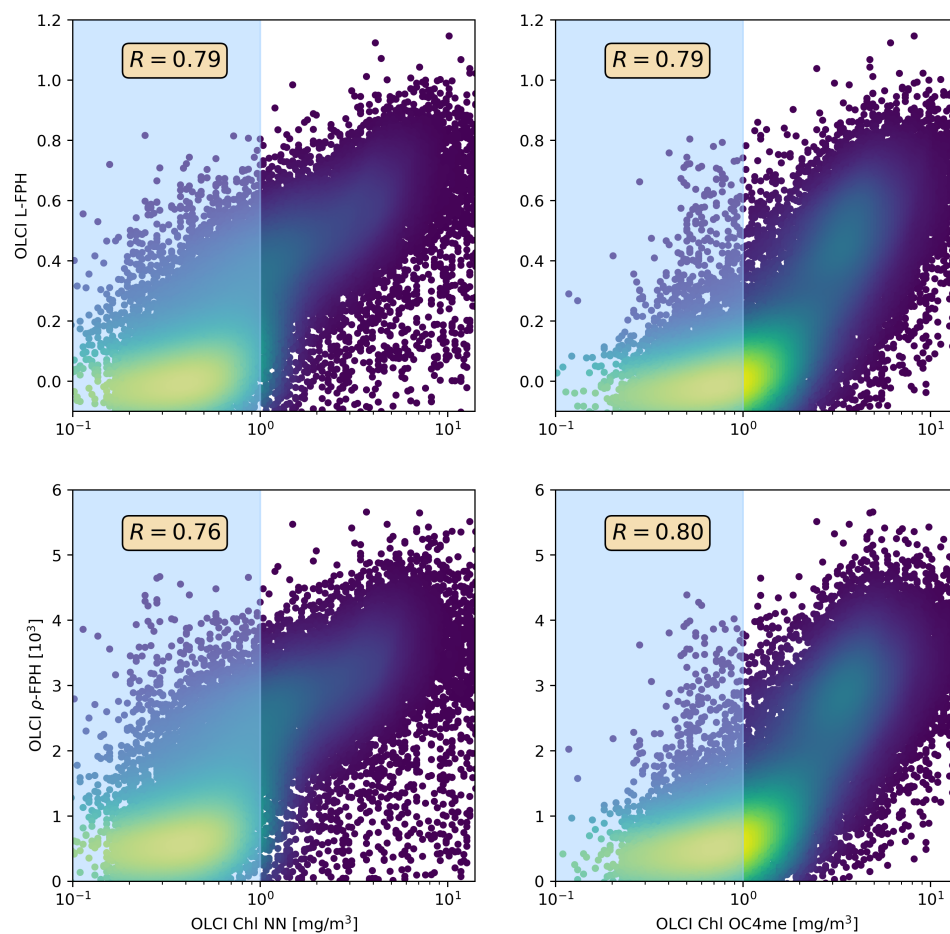


Figure 19: L-FPH and ρ_w -FPH against Chl from OC4me (upper panel) and against Chl from NN in the Barents Sea.

2.4 Validation against MODIS nFLH

nFLH from MODIS is a well-established remote sensing product and independent of our OLCI FPH products in terms of instrumental issues as well as in terms of retrieval algorithm issues. The retrieval of MODIS nFLH is described in detail in Behrenfeld et al. (2009). Note, that MODIS nFLH algorithm is based on the fully normalized water-leaving radiances, including BRDF correction, as described under Feldman, but both our OLCI products still include BRDF effects (see section 1.4.3). In the following we show three examples of a matchup comparison between OLCI and MODIS, in each case the quantitative comparison is shown in a correlation plot in Figures 22, 25 and 28 after collocation of the two, where OLCI pixels are projected on MODIS pixels. Both, MODIS nFLH and OLCI L-FPH are based on the physical radiances (the MODIS one has undergone atmospheric correction), where the spectral peak around 682 nm is expected to originate from the ocean. Accordingly both measures are expected to be very similar in absolute values. Still differences have to be expected, because MODIS nFLH characterizes the line-height of the measured spectrum at 678 nm and OLCI FPH characterizes a peak height of a peak at 682.5 nm, which might be decreased by a dip at 673.5 nm (see the description of the two algorithms, in the ATBD section 3.3.2).

2.4.1 Barents Sea, 5.7.2018, OLCI-B: 9:21am, MODIS AQUA: 8:40am

The Barents Sea is described already in sec. 2.3.3. We compare MODIS AQUA nFLH and OLCI-B FPH in the Barents Sea on the 7th of May, 2018. Fig. 20 shows the footprint of the collocated measurements of MODIS and OLCI.



Figure 20: Footprint (red rectangle) of the collocated MODIS and OLCI measurements, that are compared here.

For this comparison MODIS and OLCI differ in the overpass times by about 40 min. Fig. 21 shows the MODIS nFLH, the corresponding OLCI products are shown in Fig. 18. The patterns look by eye nearly identical. Fig. 22 shows OLCI L-FPH over MODIS nFLH and OLCI ρ_w -FPH over MODIS nFLH in a density plot. OLCI L-FPH ranges between 0 and 0.9, with the center of density at 0.6. OLCI ρ_w -FPH ranges between 0 and 5, with the center of density at 3.5. MODIS nFLH ranges between 0 and 0.9, with the center of density at 0.6. The correlation coefficient between MODIS nFLH and OLCI L-FPH as well as between MODIS nFLH and OLCI ρ_w -FPH is $R=0.81$.

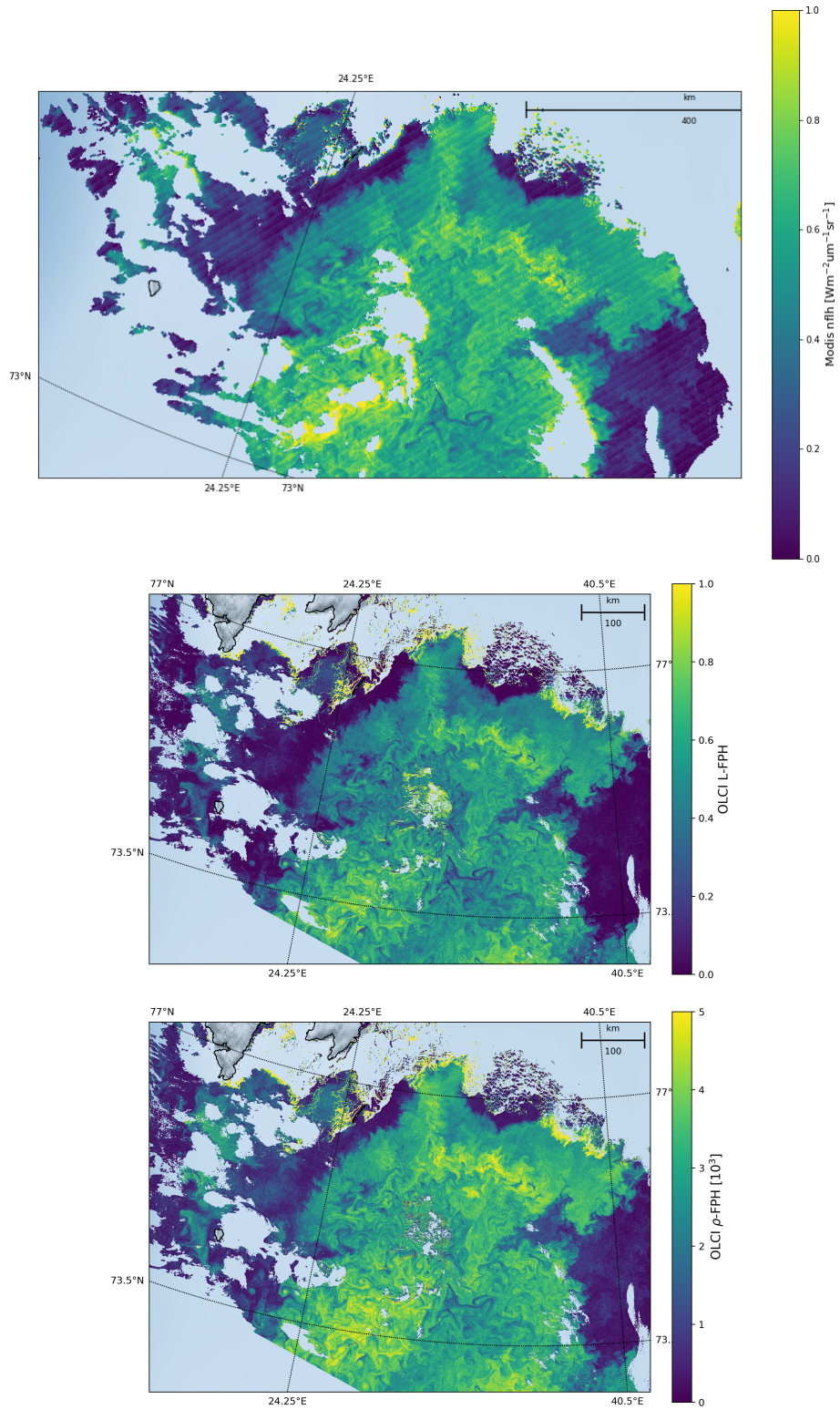


Figure 21: MODIS nFLH at 8:35-8:40 am (upper panel), OLCI L-FPH (middle panel) and ρ_w -FPH (lower panel) at 9:18 -9:21 am in the Barents Sea.

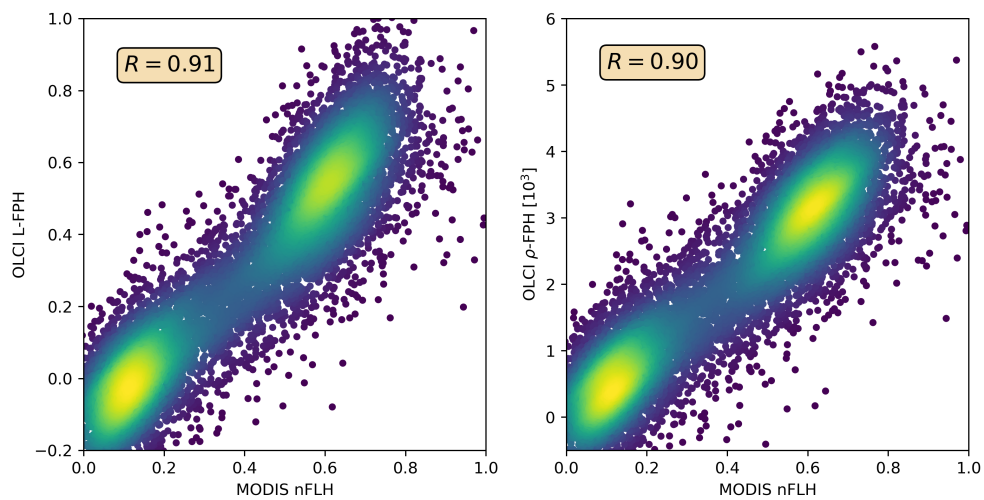


Figure 22: OLCI L-FPH over MODIS nFLH (left) and OLCI ρ_w -FPH over MODIS nFLH in the Barents Sea (right).

2.4.2 Namibian Coast, 25.11.2017, OLCI-A: 8:36am, MODIS AQUA: 12:34pm

Phytoplankton blooms are common in the coastal waters off southwest Africa where cold, nutrient-rich currents sweep north from Antarctica and interact with the coastal shelf. At the same time, the easterly trade winds push surface water away from the shore, allowing water from the ocean's floor to rise to the surface, bringing with it iron and other material (NASA, 2017). The coastal up-welling system has high seasonal and inter-annual variability in atmospheric forcing, in properties of water masses on the shelf offshore the Republic of Namibia, and in oxygen supply and demand on the shelf. In consequence, concentrations and ratios of nutrients in up-welling water have steep gradients in space and time (Hansen, 2014). We compare MODIS AQUA nFLH and OLCI-A FPH at the Namibian coast on the 25th of November, 2017. Fig. 23 shows the footprint of the collocated measurements of MODIS and OLCI.



Figure 23: Footprint (red rectangle) of the collocated MODIS and OLCI measurements, that are compared here.

For this comparison MODIS and OLCI differ in the overpass times by about 4 h. Fig. 24 shows OLCI L-FPH, OLCI ρ_w -FPH and MODIS nFLH. The main patterns look similar, but the relations in concentration from one feature to another are a bit different. Fig. 25 shows OLCI L-FPH over MODIS nFLH and OLCI ρ_w -FPH over MODIS nFLH in a density plot. There are two centers of density. OLCI L-FPH ranges between -0.6 and 0.3, with the center of density at -0.3 and -0.1. OLCI ρ_w -FPH ranges between -0.4 and 1.5, with the center of density at 0.4 and 0.8. MODIS nFLH ranges between 0 and 0.4, with the center of density at 0.1 and 0.2. The correlation coefficient between MODIS nFLH and OLCI L-FPH is $R=0.54$ and between MODIS nFLH and OLCI ρ_w -FPH $R=0.50$.

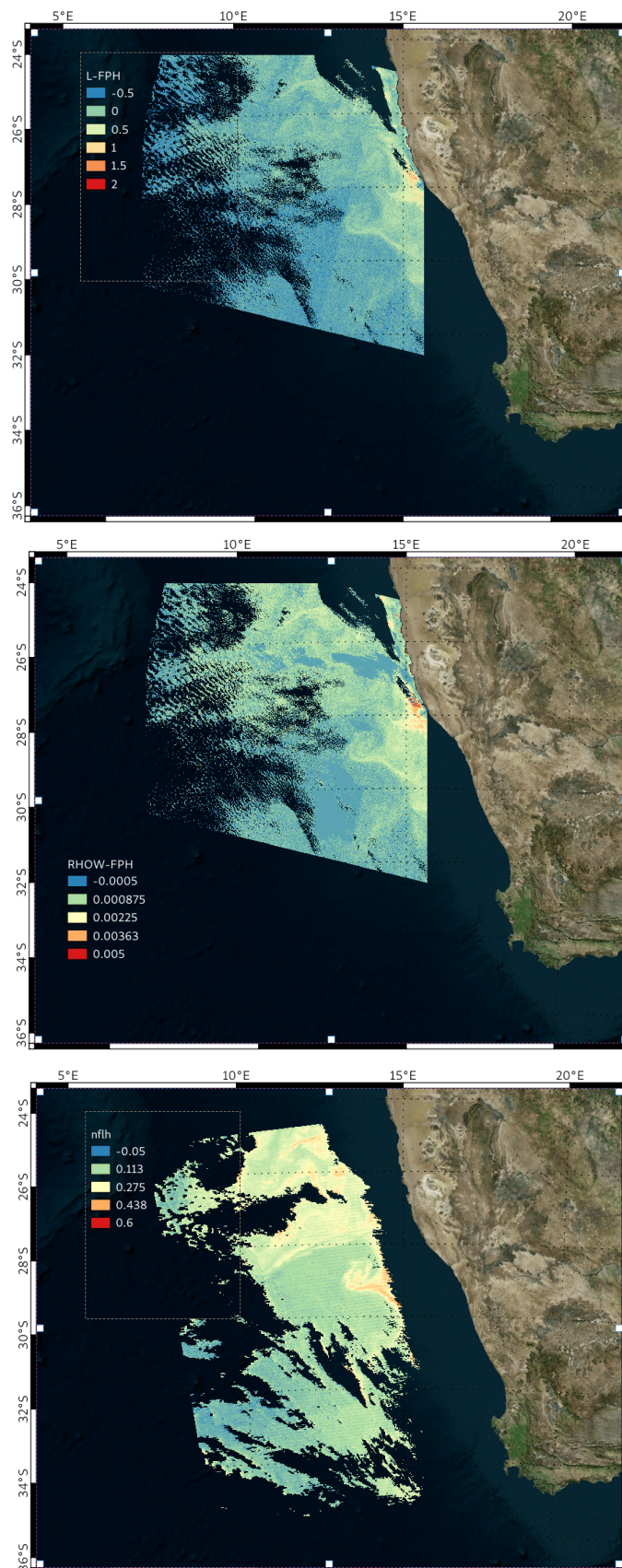


Figure 24: Upper panel: OLCI L-FPH, middle panel: OLCI ρ_w -FPH, lower panel: MODIS nFLH near the Namibian coast.

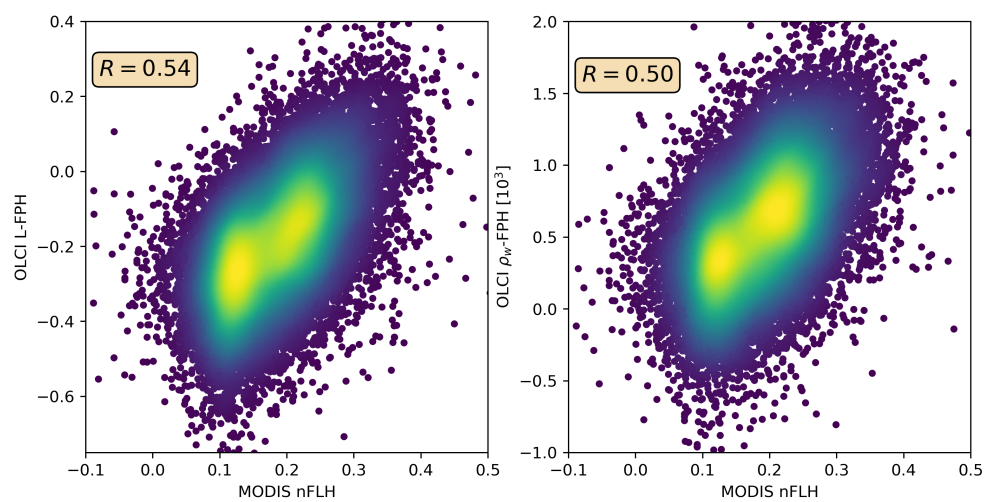


Figure 25: OLCI L-FPH over MODIS nFLH (left) and OLCI ρ_w -FPH over MODIS nFLH near the Namibian coast.

2.4.3 German Bight, 26.8.2019, OLCI-A: 10:27am, MODIS AQUA: 12:13pm

The German Bight is the southeastern bight of the North Sea bounded by the Netherlands and Germany to the south, and Denmark and Germany to the east. Several main rivers discharge into the southern North Sea, such as the river Elbe, the river Rhine, the river Weser and the river Ems. The position of the estuaries of these rivers, along with the counterclockwise residual current pattern which carries riverborne substances from west to east, favour the accumulation of eutrophying substances in the German Bight. Its coastal zone plays a major role as a recipient of large amounts of nutrient from human activities, including effluents, agriculture runoff, and municipal sewage (Schlüter, 2010). We compare MODIS AQUA nFLH and OLCI-A FPH in the German Bight on the 26th of August, 2019. Fig. 26 shows the footprint of the collocated measurements of MODIS and OLCI. For this comparison MODIS and OLCI differ in the overpass times by about



Figure 26: Footprint (red rectangle) of the collocated MODIS and OLCI measurements, that are compared here.

2 h. Fig. 27 shows OLCI L-FPH, OLCI ρ_w -FPH and MODIS nFLH. The patterns look nearly identical. Fig. 28 shows OLCI L-FPH over MODIS nFLH and OLCI ρ_w -FPH over MODIS nFLH in a density plot. OLCI L-FPH ranges between -0.35 and 0.1, with the center of density at -0.2. OLCI ρ_w -FPH ranges between -0.25 and 1, with the center of density at 0.1. MODIS nFLH ranges between -0.05 and 0.2, with the center of density at 0.03. The correlation coefficient between MODIS nFLH and OLCI L-FPH is $R=0.84$ and between MODIS nFLH and OLCI ρ_w -FPH $R=0.87$.

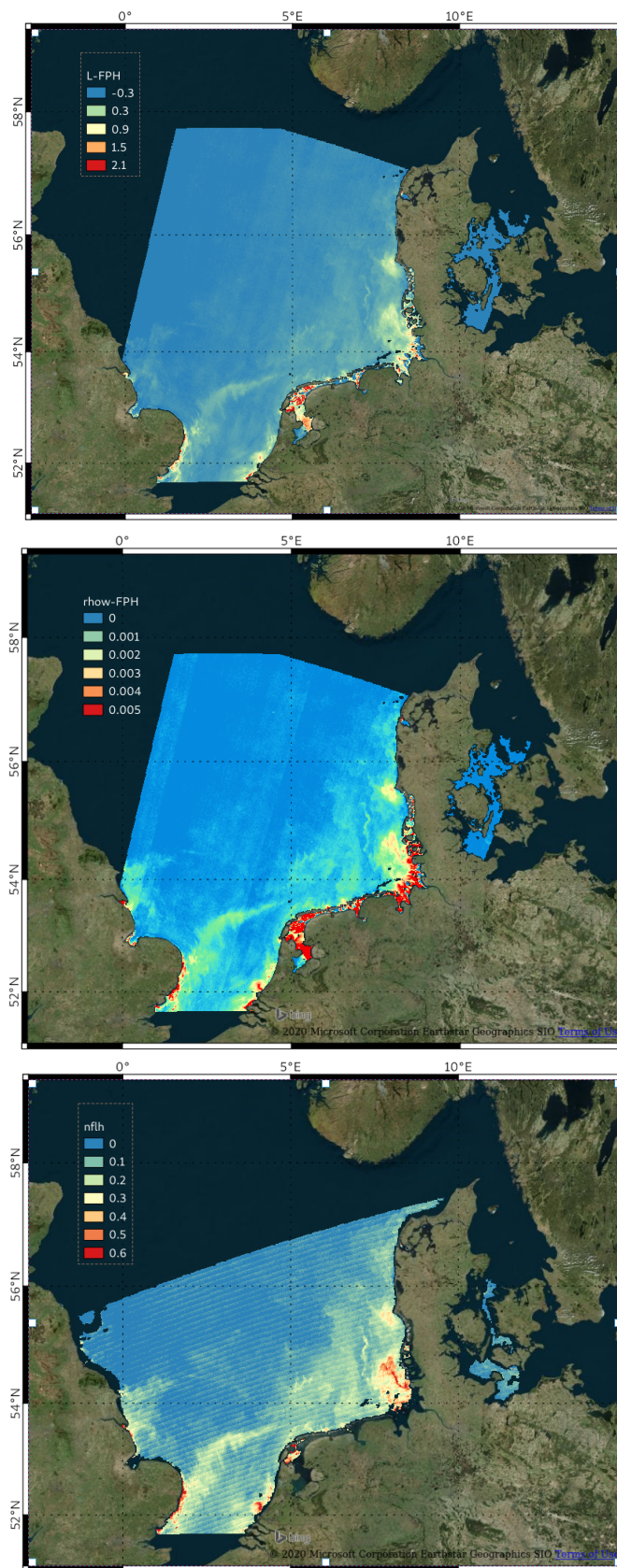


Figure 27: Upper panel: OLCI L-FPH, middle panel: OLCI ρ_w -FPH, lower panel: MODIS nFLH in the German Bight.

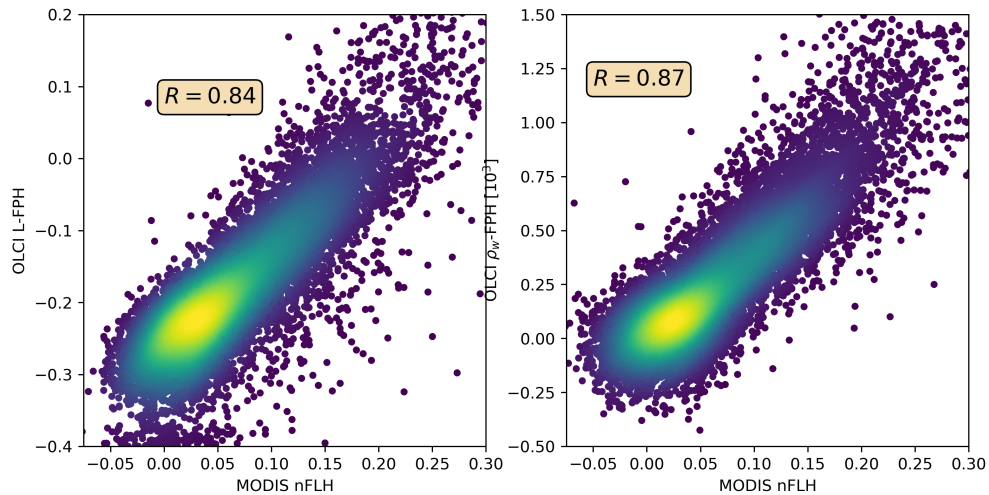


Figure 28: OLCI L-FPH over MODIS nFLH (left) and OLCI ρ_w -FPH over MODIS nFLH for the German Bight.

2.4.4 Conclusion on the comparison to MODIS nFLH

The overall patterns of OLCI L-FPH and ρ_w -FPH are so alike that the correlation coefficient to MODIS is in both cases nearly the same. Due to the physical units, absolute values of L-FPH are more comparable to MODIS, than the ones of ρ_w -FPH, while the negative offset of ρ_w -FPH is more comparable to MODIS, than the one from L-FPH. This is most likely due to the atmospheric correction, which is applied as well to MODIS nLw as to OLCI ρ_w . The correlation is very good for the Barents Sea and the German Bight example and less good for the Namibian coast, where the time gap of 4h is probably too large.

2.5 Validation on simulated data

Radiative transfer simulations are performed for developing and testing the OC-Fluo algorithm. As described before in section 1.2 the emitted fluorescence quantum in nature depends on many factors, like the quantum yield, the chlorophyll concentration, illumination, etc., which are not known, or at least not accurately known. A synthetic approach, like the one described here is the only way to control all influences on the fluorescence signal. In the RTM fluorescence is a strictly increasing function of the chlorophyll concentration. In case the mathematical function is able to capture the fluorescence peak from OLCI spectrally convoluted reflectances the retrieved FPH should be a strictly increasing function to input chlorophyll.

2.5.1 The RTM MOMO and the bio-optical model

The simulations are performed using the vector version of MOMO (Fell and Fischer (2001), Hollstein and Fischer (2012)). Here a horizontal homogeneous atmosphere and ocean consisting of layers with vertical uniform optical properties are assumed. The upward and downward directed light field is calculated at all inter layer boundaries and for all solar positions. The azimuthal dependence of the light field is internally expressed as Fourier series and reconstructed at equidistant distributed azimuth angles. The model is operated by several input files which govern the height profile of atmosphere and ocean, the scatterers, the absorbers and the atmosphere ocean interface. For this set of simulations a water body was implemented with 20 layers of 1m thickness and is assumed to be homogeneous with an equal distribution of constituents (phytoplankton and CDOM) in each layer. The absorption coefficient of pure sea water

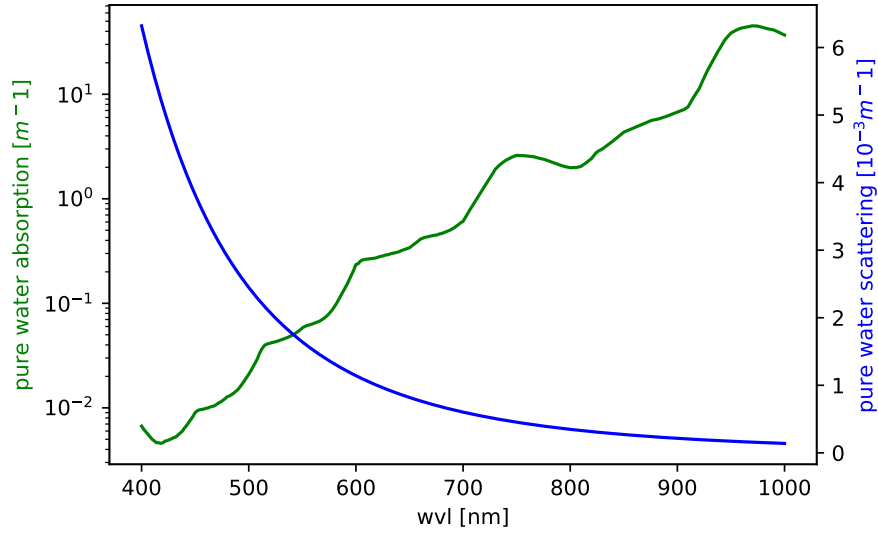


Figure 29: Spectral scattering (blue) and absorption (green) of pure seawater for salinity $S=20$ PSU and temperature $T=20^{\circ}\text{C}$ (Röttgers et al., 2010).

Table 3: Input IOPS for MOMO

IOP [1/m]	0.04	0.4	0.8	1.0	1.4	1.8	3.0	5.0	7.0
concentration [mg/m ³]	0.84	8.4	16.8	21	29.4	37.8	63	105	147

(see Fig. 29) is a result from the ESA project WATERRADIANCE (Röttgers et al., 2010) as a linear expansion with coefficients for salinity and temperature. The volume scattering coefficient of sea water is the sum of contributions from density fluctuations and concentration fluctuations and has been discussed in Zhang and Hu (2009). Fig. 29 shows the absorption and scattering coefficients for salinity $S=20$ PSU and temperature $T=20^{\circ}\text{C}$. We apply a bio-optical model, where chlorophyll concentration governs as well chlorophyll absorption coupled to chlorophyll fluorescence with a quantum yield of 0.03, as CDOM absorption and scattering (Bricaud et al. (2010)). The chlorophyll-a extinction coefficient and the corresponding single scattering albedo control the amplitude and spectral signature of phytoplankton. A normalized chlorophyll-a absorption spectrum is scaled at 440 nm in order to calculate the absorption spectrum $a_{ph}(\lambda)$ for different phytoplankton amounts. The single scattering albedo ω_0 at 440 nm is set to 0.68 (J. Fischer, pers. communication) to calculate spectral phytoplankton scattering $b_{ph}(\lambda)$ with

$$b_{ph}(\lambda) = a_{ph}\omega_0\lambda/(1-\omega_0) \quad (3)$$

Phytoplankton scattering is constrained by a phase function measured from Petzold (1972) which can be mathematically expressed with the Fournier-Forand function with a backscattering ratio of 0.01986. The simulated data cover a large range of chlorophyll concentrations (see table 3), which are governed by the absorption coefficients at 440 nm from 0.004 m^{-1} to 7 m^{-1} . The simulations are performed in 1 nm resolution from 390 nm to 740 nm.

Technically the fluorescence is simulated in two subsequent model runs. In the first run the energy that is absorbed by chlorophyll (photosynthetically active radiation, PAR) is calculated and in the second model run this energy is multiplied by the quantum efficiency of 0.03 and implemented as a gaussian shaped peak source, centered at 682.5 nm and halfwidth of 25 nm.

2.5.2 Calculation of ρ_w and convolution to OLCI and MERIS spectral response function

The ρ_w is not a direct model output, but is derived from up- and downward radiances (L_{\uparrow} , L_{\downarrow}) and irradiances (E_{\uparrow} , E_{\downarrow}) just above water surface:

$$\rho_w(\theta, \phi, \lambda) = \pi L_w(\theta, \phi, \lambda) / E_{\downarrow}(\lambda) \quad (4)$$

where the water-leaving radiance L_w is calculated from

$$L_w(\theta, \phi, \lambda) = (L_{\uparrow}(\theta, \phi, \lambda) - L_{black}(\theta, \phi, \lambda)) / E_{\downarrow}(\lambda) \quad (5)$$

and L_{black} is L_{\uparrow} from only the ocean surface. This is realised in the model, by implementing a very thin water body with a black surface below.

The resulting ρ_w is shown in Fig. 30 in 1 nm resolution and in OCLI's spectral resolution within the spectral domain of the OCLI bands Oa8 to Oa12. The MERIS band setting, which is a subset of OLCIS bands is included.

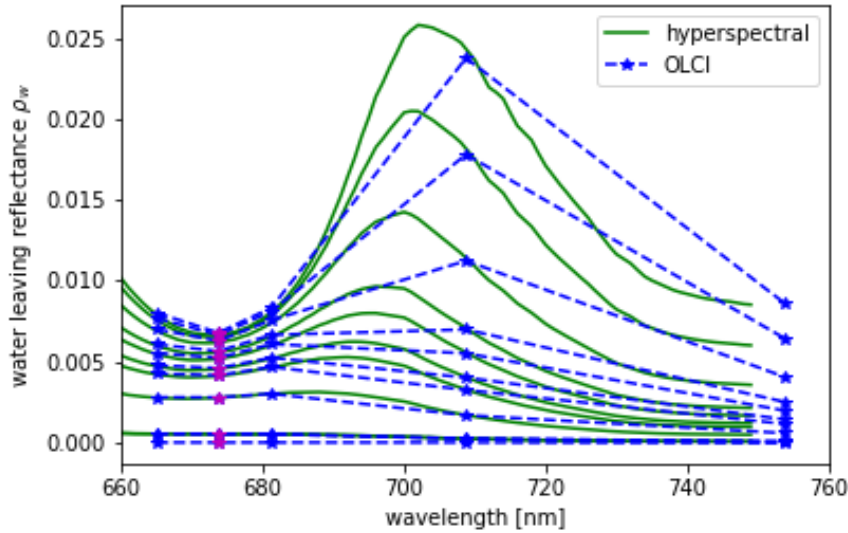


Figure 30: Hyperspectral (green) ρ_w from RTM and its convolution to OLCI (blue) spectral resolution for $\theta_S=48^\circ$, $\theta_V=34^\circ$, $\phi_V=90^\circ$ and chlorophyll concentrations given in table 3, while the lowest spectrum is the one with the lowest chlorophyll concentration. Band Oa09 from OLCI which is additional to MERIS bands is shown in magenta.

We apply the proposed algorithm to the convoluted remote sensing reflectances. The upper panel in Fig. 31 shows ρ_w -FPH retrieved from synthetic spectra over Chl, calculated from the simulations input. Results are shown for OLCI and MERIS band setting, while the MERIS results are produced by just excluding band Oa9 from the retrieval. Both band settings give an unambiguous and very similar relationship. The lower panel in Fig. 31 shows the relative difference of ρ_w -FPH retrieved from synthetic spectra in OLCI and MERIS band setting over chlorophyll. Up to 40mg/m³ chlorophyll the difference is less than 4% and even for very high concentrations up to 140mg/m³ it does not exceed 10%. This means the algorithm can be also applied to MERIS measurements and the results can be directly compared to each other. Consequently long time series of nearly twenty years of FPH could be generated and analysed. In order to investigate the reasons for the similarity of OLCI and MERIS results, we illustrate the extracted spectral components. The division into the spectral components is shown in Fig. 32 for OLCI and for only MERIS bands applied to a ρ_w -spectrum with low and with high chlorophyll. For low chlorophyll concentrations the spectral model seems to reproduce the simulated spectrum perfectly

as well for MERIS as for the OLCI band setting. For higher concentrations the additional band Oa9 pulls the reproduced spectrum a bit down, which leads to a slightly lower FPH. The fact that the reproduced spectrum is slightly off the measured bands indicates that for extremely high chlorophyll concentrations the model could be adjusted to a spectrally even more complex behaviour.

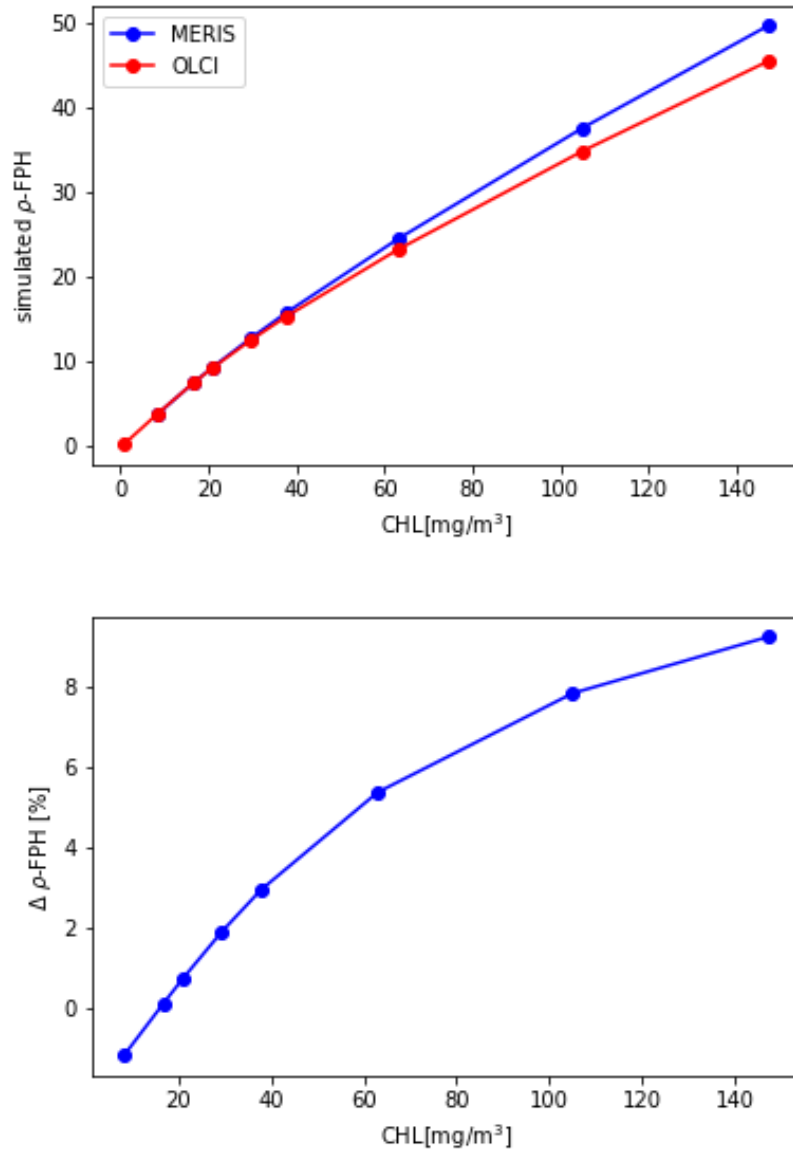


Figure 31: ρ_w -FPH retrieved from synthetic spectra over chlorophyll, which was input for the RTM for OLCI (red) and for MERIS (blue) band setting (upper panel). Relative difference between ρ_w -FPH retrieved from synthetic spectra in OLCI and MERIS band setting over chlorophyll (lower panel).

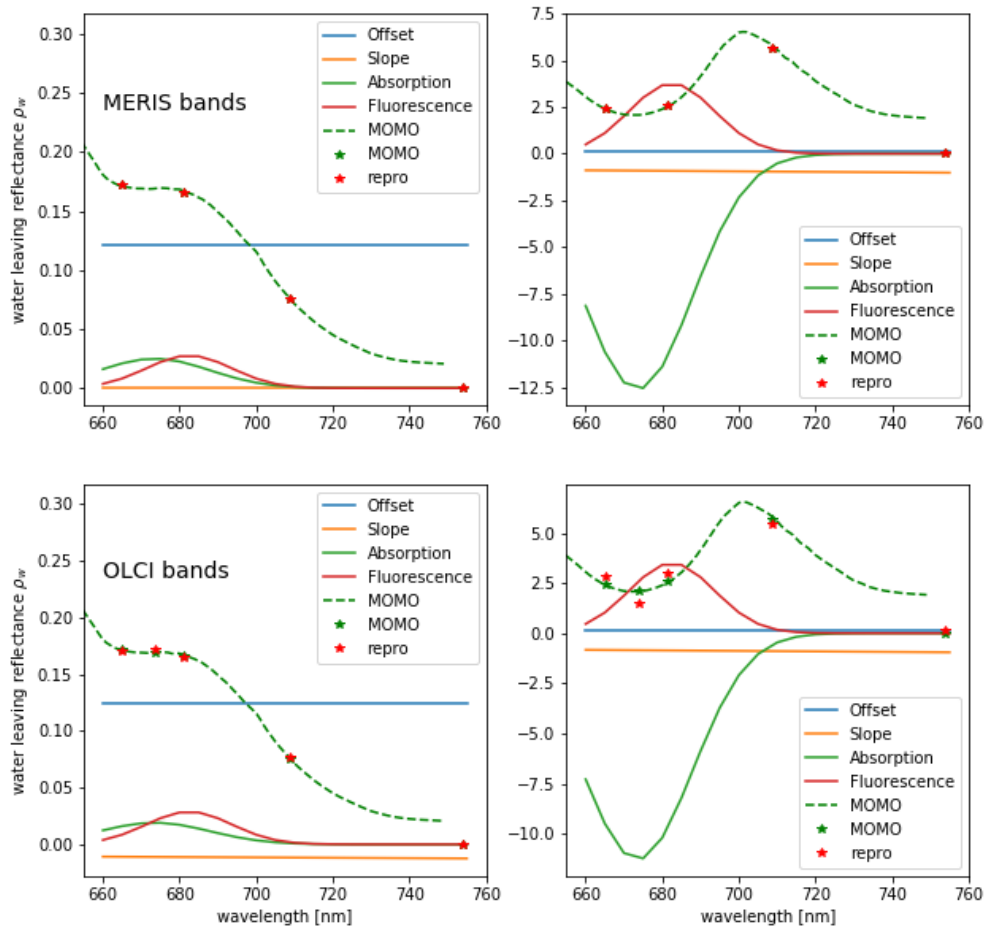


Figure 32: Components found by the retrieval of ρ_w -FPH applied to a ρ_w -spectrum with low (left panels) and with high (right panels) chlorophyll for MERIS (upper panel) and for OLCI (lower panel) band setting.

2.5.3 BRDF effect

In order to investigate the impact of the non lambertian BRDF of the sea surface on the Fluorescence product, we calculate from RTM the exactly normalized water-leaving reflectance ρ_w^N , which is $\rho_w(\theta_S, \theta_V, \lambda)$ with $\theta_S=0$ and $\theta_V=0$. (see sec. 1.4.3) through:

$$\rho_w(0, 0, \lambda) = \pi L_w(0, 0, \lambda) / E \downarrow(\lambda) \quad (6)$$

The water-leaving radiance L_w is calculated from the difference of the upward radiance just above the surface of the modeled water body and the same quantity above a black (non-reflective) water body. This step removes the reflection at the water surface.

$$L_w(0, 0, \lambda) = (L \uparrow(0, 0, \lambda) - L_{black}(0, 0, \lambda)) / E \downarrow(\lambda) \quad (7)$$

Fig. 33 shows ρ_w^N (solid) and $\rho_w(\theta_S, \theta_V, \lambda)$ with $\theta_S=48^\circ$, $\theta_V=34^\circ$, $\phi_V=90^\circ$ (dashed) for the different chlorophyll concentrations given in table 3 (different colours). There is a about 0.05 offset between both geometries, while the exactly normalized ρ_w is brighter. This offset can be captured in the retrieval by the fitted offset. However the peak height is larger for the not normalized spectrum.

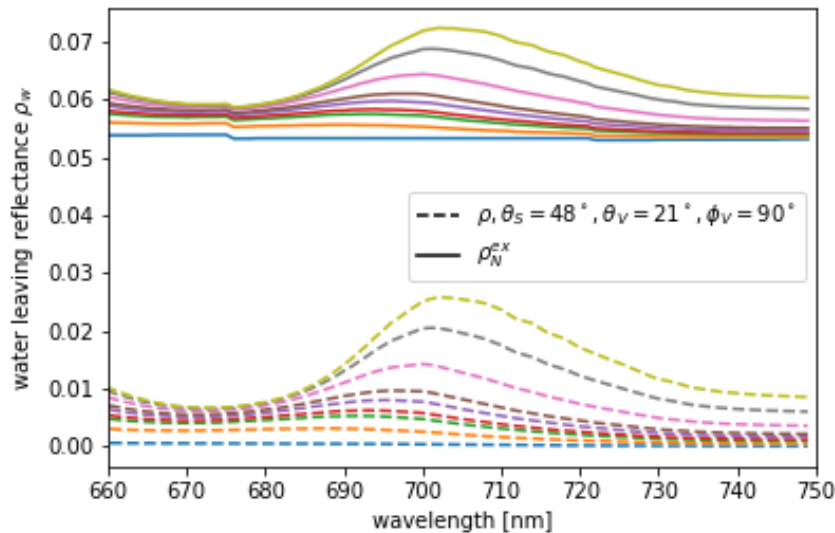


Figure 33: Hyperspectral ρ_w^N (solid) and $\rho_w(\theta_S, \theta_V, \lambda)$ with $\theta_S=48^\circ$, $\theta_V=34^\circ$, $\phi_V=90^\circ$ (dashed) for the different chlorophyll concentrations given in table 3 (different colours).

From the simulated ρ_w , ρ_w -FPH is retrieved for both geometries. The results are shown in Fig. 35. The relative difference is shown in Fig. 34 and gets stronger with increasing chlorophyll concentration. It exceeds 20% for the highest chlorophyll concentration (147 mg/m³). For moderate chlorophyll concentrations the relative difference is around 16%.

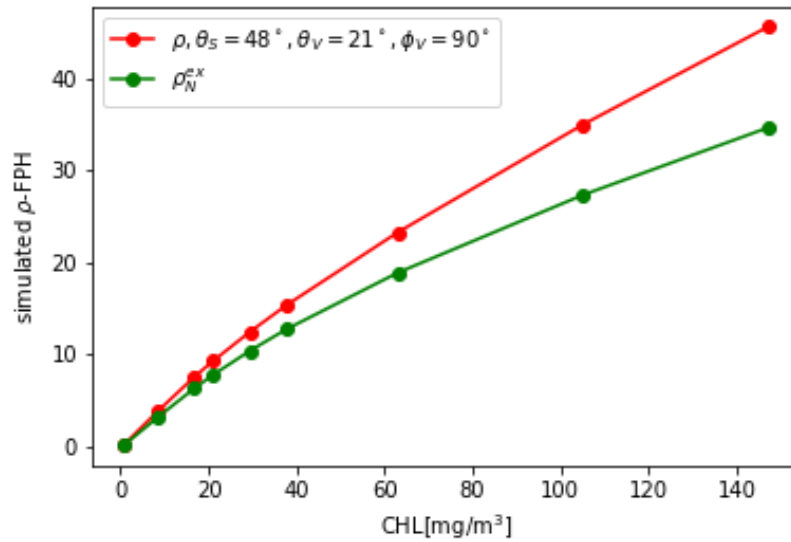


Figure 34: ρ_w -FPH retrieved from OLCI-resolved synthetic spectra in nadir-nadir geometry (green) and for $\theta_S=48^\circ$, $\theta_V=34^\circ$, $\phi_V=90^\circ$ over chlorophyll, which was input for the RTM.

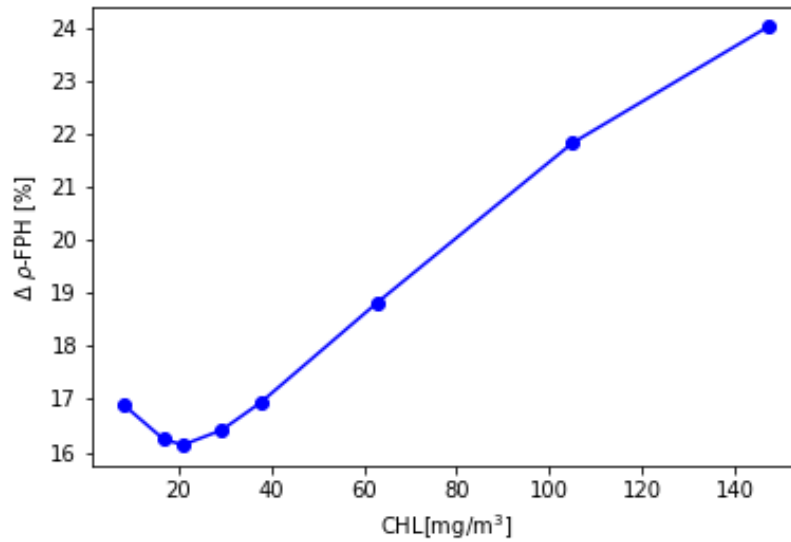


Figure 35: Relative difference between ρ_w -FPH from retrieved from $\rho_w(\theta_S, \theta_V, \lambda)$ with $\theta_S=48^\circ$, $\theta_V=34^\circ$, $\phi_V=90^\circ$ and ρ_w^N over chlorophyll.

2.5.4 Conclusion on FPH simulations

With RTM we produce spectrally high resolved ρ_w spectra that are convoluted to OLCI spectral resolution and analyzed by the OC-Fluo algorithm. The resulting ρ_w -FPH is a strictly increasing function of the input chlorophyll, which is governing the fluorescence in the model. From this we conclude, that FPH is a good measure of the fluorescence. Furthermore the resulting relationship between FPH and chlorophyll produced from MERIS band setting is very similar, with a difference below 10% throughout the concentration range. Therefore the algorithm is applicable to MERIS measurements and results are directly transferable. With our RTM we also studied the effect of the BRDF on the retrieved FPH. The relative difference between different viewing geometries exceeds 20% for high chlorophyll concentrations.

3 Limitations

The sensitivity range of the algorithm is determined by the sensitivity of the measurements towards the fluorescence signal and the ability of algorithm to retrieve it. From our fluorescence to chlorophyll comparisons and in agreement with earlier assessments (see section 1.3), we estimate the sensitivity range of the processor to chlorophyll $> 1\text{mg/m}^3$ which corresponds to $L\text{-FPH} > 0 \text{ mWm}^{-2}\text{sr}^{-1}\text{nm}^{-1}$ and $\rho_w\text{-FPH} > 0.1$. This is based on the observation that below this threshold data can become noisy and L-FPH values become negative. This sensitivity threshold will also be subject to further investigations.

Parameter	Chlorophyll	L-FPH	$\rho_w\text{-FPH}$
sensitivity threshold	1mg/m^3	$0 \text{ mWm}^{-2}\text{sr}^{-1}\text{nm}^{-1}$	0.1

Table 4: Sensitivity thresholds for the output parameter of the OC-Fluo algorithm.

4 Conclusions

On behalf of the validation of the OLCI L-FPH and $\rho_w\text{-FPH}$ product we followed different approaches. Both products show a good correlation to in-situ measured and remotely sensed chlorophyll, if the chlorophyll concentration is higher than 1mg/m^3 . For lower chlorophyll concentrations the scatter is large and especially L-FPH values become negative. From this we can conclude, that our FPH product is a good tracer for chlorophyll and especially for high values therein. This feature has to be studied in more detail, in particular atmospheric impacts, even when there are small their might have an impact on small fluorescence signals.

Even though OLCI FPH and MODIS nFLH are not exactly the same measures, there is a very high correlation between both.

From RTM we can conclude, that FPH is a strictly increasing function of the fluorescence magnitude. Furthermore the algorithm is applicable to MERIS measurements and results are directly transferable. With relative differences up to 20% for high chlorophyll concentrations, the BRDF effect is an open issue.

References

- M. Babin, A. Morel, and B. Gentili. Remote sensing of sea surface Sun-induced chlorophyll fluorescence: consequences of natural variations in the optical characteristics of phytoplankton and the quantum yield of chlorophyll a fluorescence. *International Journal of Remote Sensing*, 17(12):2417–2448, 8 1996. ISSN 0143-1161. doi: 10.1080/01431169608948781. URL <https://www.tandfonline.com/doi/full/10.1080/01431169608948781>.
- M. J. Behrenfeld, T. K. Westberry, E. S. Boss, R. T. O’Malley, D. A. Siegel, J. D. Wiggert, B. A. Franz, C. R. McClain, G. C. Feldman, S. C. Doney, J. K. Moore, G. Dall’Olmo, A. J. Milligan, I. Lima, and N. Mahowald. Satellite-detected fluorescence reveals global physiology of ocean phytoplankton. *Biogeosciences*, 6(5):779–794, 5 2009. ISSN 1726-4189. doi: 10.5194/bg-6-779-2009. URL <http://www.biogeosciences.net/6/779/2009/>.
- C. E. Binding, T. A. Greenberg, J. H. Jerome, R. P. Bukata, and G. Letourneau. An assessment of MERIS algal products during an intense bloom in Lake of the Woods. *Journal of Plankton Research*, 33(5):793–806, 5 2011. ISSN 0142-7873. doi: 10.1093/plankt/fbq133. URL <https://academic.oup.com/plankt/article-lookup/doi/10.1093/plankt/fbq133>.
- G. A. Borstad, H. R. Edel, J. Gower, and A. B. Hollinger. Analysis of test and flight data from the Fluorescence Line Imager. Technical report, 1987. URL <http://publications.gc.ca/site/eng/9.816405/publication.html>.

- A. Bricaud, M. Babin, H. Claustre, J. Ras, and F. Tièche. Light absorption properties and absorption budget of Southeast Pacific waters. *Journal of Geophysical Research: Oceans*, 115(8):1–19, 2010. ISSN 21699291. doi: 10.1029/2009JC005517.
- C. Brockmann, R. Doerffer, P. Marco, K. Stelzer, S. Embacher, and A. Ruescas. Evolution Of The C2RCC Neural Network For Sentinel 2 and 3 For The Retrieval of Ocean. *Proc. 'Living Planet Symposium 2016', Prague, Czech Republic, 9–13 May 2016 (ESA SP-740, August 2016)*, 2016(August): 9–13, 2016.
- EUMETSAT. Recommendations for Sentinel-3 OLCI Ocean Colour product validations in comparison with in situ measurements – Matchup Protocols. pages 1–10, 2019.
- Eumetsat Ocean Color In-situ Database. Ocean Colour In-Situ Database, 2019. URL <https://ocdb.eumetsat.int/>.
- P. Falkowski and D. A. Kiefer. Chlorophyll fluorescence in phytoplankton: relationship to photosynthesis and biomass. *Journal of Plankton Research*, 7(5):715–731, 1985. ISSN 0142-7873. doi: 10.1093/plankt/7.5.715. URL <https://academic.oup.com/plankt/article-lookup/doi/10.1093/plankt/7.5.715>.
- P. G. Falkowski, H. Lin, and M. Y. Gorbunov. What limits photosynthetic energy conversion efficiency in nature? Lessons from the oceans. *Philosophical Transactions of the Royal Society B: Biological Sciences*, 372(1730):20160376, 9 2017. ISSN 0962-8436. doi: 10.1098/rstb.2016.0376. URL <http://www.ncbi.nlm.nih.gov/pubmed/28808095><http://www.pubmedcentral.nih.gov/articlerender.fcgi?artid=PMC5566876><http://rstb.royalsocietypublishing.org/lookup/doi/10.1098/rstb.2016.0376>.
- G. C. Feldman. NASA's OceanColor Web. URL oceancolor.gsfs.nasa.gov.
- F. Fell and J. Fischer. Numerical simulation of the light field in the atmosphere-ocean system using the matrix-operator method. *Journal of Quantitative Spectroscopy and Radiative Transfer*, 69(3):351–388, 2001. ISSN 00224073. doi: 10.1016/S0022-4073(00)00089-3.
- J. Fischer and U. Kronfeld. Sun-stimulated chlorophyll fluorescence 1: Influence of oceanic properties. *International Journal of Remote Sensing*, 11(12):2125–2147, 1990. ISSN 13665901. doi: 10.1080/01431169008955166.
- H. Gons, M. Auer, S. E. R. S. o. Environment, and U. 2008. MERIS satellite chlorophyll mapping of oligotrophic and eutrophic waters in the Laurentian Great Lakes. *Elsevier*, 2008. URL <https://www.sciencedirect.com/science/article/pii/S0034425708002083>.
- H. R. Gordon and K. J. Voss. MODIS Normalized Water-leaving Radiance Algorithm Theoretical Basis Document (MOD 18). Technical Report Mod 18, 1999.
- J. Gower. A simpler picture of satellite chlorophyll fluorescence. *Remote Sensing Letters*, 5(6):583–589, 6 2014. ISSN 2150-704X. doi: 10.1080/2150704X.2014.940630. URL <http://www.tandfonline.com/doi/abs/10.1080/2150704X.2014.940630>.
- J. Gower and S. King. Validation of chlorophyll fluorescence derived from MERIS on the west coast of Canada. *International Journal of Remote Sensing*, 28(3-4):625–635, 2007a. ISSN 01431161. doi: 10.1080/01431160600821010.
- J. Gower and S. King. Validation of chlorophyll fluorescence derived from MERIS on the west coast of Canada. *International Journal of Remote Sensing*, 28(3-4):625–635, 2 2007b. ISSN 0143-1161. doi: 10.1080/01431160600821010. URL <https://www.tandfonline.com/doi/full/10.1080/01431160600821010>.
- A. L. I. f. B. S. Hansen. podcampus | Phytoplankton analysis off the coast of Namibia, 2014. URL <https://www.podcampus.de/nodes/QVKNA>.

- F. E. Hoge, P. E. Lyon, R. N. Swift, J. K. Yungel, M. R. Abbott, R. M. Letelier, and W. E. Esaias. Validation of Terra-MODIS phytoplankton chlorophyll fluorescence line height I Initial airborne lidar results. *Applied Optics*, 42(15):2767, 5 2003. ISSN 0003-6935. doi: 10.1364/AO.42.002767. URL <https://www.osapublishing.org/abstract.cfm?URI=ao-42-15-2767>.
- A. Hollstein and J. Fischer. Radiative transfer solutions for coupled atmosphere ocean systems using the matrix operator technique. *Journal of Quantitative Spectroscopy and Radiative Transfer*, 113(7):536–548, 2012. ISSN 00224073. doi: 10.1016/j.jqsrt.2012.01.010.
- C. Hu, F. E. Muller-Karger, C. J. Taylor, K. L. Carder, C. Kelble, E. Johns, and C. A. Heil. Red tide detection and tracing using MODIS fluorescence data: A regional example in SW Florida coastal waters. *Remote Sensing of Environment*, 97(3):311–321, 8 2005. ISSN 0034-4257. doi: 10.1016/j.RSE.2005.05.013. URL <https://www.sciencedirect.com/science/article/abs/pii/S0034425705001598>.
- Y. Huot, C. A. Brown, and J. J. Cullen. New algorithms for MODIS sun-induced chlorophyll fluorescence and a comparison with present data products. *Limnology and Oceanography: Methods*, 3(2):108–130, 2 2005. ISSN 15415856. doi: 10.4319/lom.2005.3.108. URL <http://doi.wiley.com/10.4319/lom.2005.3.108>.
- I. Ioannou, J. Zhou, A. Gilerson, B. Gross, F. Moshary, and S. Ahmed. New algorithm for MODIS chlorophyll fluorescence height retrieval: performance and comparison with the current product. page 747309, 9 2009. doi: 10.1117/12.830630. URL <http://proceedings.spiedigitallibrary.org/proceeding.aspx?doi=10.1117/12.830630>.
- S. Jeffrey and G. Humphrey. New spectrophotometric equations for determining chlorophylls a, b, c1 and c2 in higher plants, algae and natural phytoplankton. *Biochimie und Physiologie der Pflanzen*, 167(2):191–194, 1975. ISSN 00153796. doi: 10.1016/S0015-3796(17)30778-3. URL [http://dx.doi.org/10.1016/S0015-3796\(17\)30778-3](http://dx.doi.org/10.1016/S0015-3796(17)30778-3).
- D. A. Kiefer. Fluorescence properties of natural phytoplankton populations. *Marine Biology*, 22(3):263–269, 1973. ISSN 0025-3162. doi: 10.1007/BF00389180. URL <http://link.springer.com/10.1007/BF00389180>.
- R. Letelier. An analysis of chlorophyll fluorescence algorithms for the moderate resolution imaging spectrometer (MODIS). *Remote Sensing of Environment*, 58(2):215–223, 11 1996. ISSN 00344257. doi: 10.1016/S0034-4257(96)00073-9. URL <http://linkinghub.elsevier.com/retrieve/pii/S0034425796000739>.
- H. Lin, F. I. Kuzminov, J. Park, S. Lee, P. G. Falkowski, and M. Y. Gorbunov. Phytoplankton. The fate of photons absorbed by phytoplankton in the global ocean. *Science (New York, N.Y.)*, 351(6270):264–7, 1 2016. ISSN 1095-9203. doi: 10.1126/science.aab2213. URL <http://www.ncbi.nlm.nih.gov/pubmed/26743625>.
- C. Mazeran, C. B. Brockmann, K. Ruddick, K. Voss, and F. Zagolski. Requirements for Copernicus Ocean Colour Vicarious Calibration Infrastructure. Number July, 2017.
- A. Morel, B. Gentili, H. Claustre, M. Babin, A. Bricaud, J. Ras, and F. Tièche. Optical properties of the “clearest” natural waters. *Limnology and Oceanography*, 52(1):217–229, 2007. ISSN 00243590. doi: 10.4319/lo.2007.52.1.0217.
- M. J. Moreno-Madrinán and A. M. Fischer. Performance of the MODIS FLH algorithm in estuarine waters: a multi-year (2003–2010) analysis from Tampa Bay, Florida (USA). *International Journal of Remote Sensing*, 34(19):6467–6483, 10 2013. ISSN 0143-1161. doi: 10.1080/01431161.2013.804227. URL <https://www.tandfonline.com/doi/full/10.1080/01431161.2013.804227>.
- NASA. Phytoplankton Bloom off Namibia, 2017. URL https://www.nasa.gov/multimedia/imagegallery/image_feature_975.html.

- T. Petzold. Volume Scattering Functions for Selected Ocean Waters. *Scripps Inst. Oceanogr.*, (3): 72–78, 1972. ISSN 1936-900X. doi: 10.5811/westjem.2013.7.18472. URL <http://oai.dtic.mil/oai/oai?verb=getRecord&metadataPrefix=html&identifier=AD0753474>.
- R. Röttgers, R. Doerffer, D. Mckee, and W. Schönfeld. Pure water spectral absorption, scattering, and real part of refractive index model Algorithm Technical Basis Document - Draft. Technical report, 2010.
- M. H. Schlüter. *Investigating environmental changes in the southern North Sea: a combined statistical assessment of climatic and biogeochemical long-term time series*. PhD thesis, Hamburg, 2010.
- P. J. Werdell, S. Bailey, G. Fargion, C. Pietras, K. Knobelspiesse, G. Feidman, and C. McClain. Unique data repository facilitates ocean color satellite validation. *Eos*, 84(38):2002–2004, 2003. ISSN 00963941. doi: 10.1029/2003EO380001.
- X. G. Xing, D. Z. Zhao, Y. G. Liu, J. H. Yang, P. Xiu, and L. Wang. An overview of remote sensing of chlorophyll fluorescence. *Ocean Science Journal*, 42(1):49–59, 2007. ISSN 17385261. doi: 10.1007/BF03020910.
- X. Zhang and L. Hu. Scattering by pure seawater at high salinity. *Optics Express*, 17(15):12685, 2009. ISSN 1094-4087. doi: 10.1364/OE.17.012685. URL <https://www.osapublishing.org/oe/abstract.cfm?uri=oe-17-15-12685>.